Ca' Foscari
University
of Venice

Master's Degree Programme

Environmental Sciences:

Global Environmental Changes

Final Thesis

Paleofire activity reconstruction in the Tibetan Plateau

Supervisor
Prof. Dr. Dario Battistel

Assistant supervisor
Alice Callegaro

MSc student
Felipe Matsubara Pereira
Matriculation Number 855535

Academic Year
2015 / 2016

ABSTRACT

A 435 cm long sediment core, covering the last 10.9 thousand years before present (ky BP) and collected from an alpine lake sediment archive on the southeastern Tibetan Plateau (Paru Co) was analysed for monosaccharide anhydrides (MAs) and polycyclic aromatic hydrocarbons (PAHs). This multi-proxy approach and the comparison with other proxies showed that fire has been present since the early Holocene, as a consequence of a shift from cold-dry to warm-wet conditions causing, e.g. decreasing ice-sheet size and vegetation changes, due to a strong solar radiation in the northern hemisphere and an intense presence of the Indian Summer Monsoon (ISM) until ~7 ky BP. The mid-late Holocene was marked by a decrease in solar insolation reintroducing the cooler and drier climate at the Tibetan Plateau. Paru Co's hydrogen isotopic measurements of leaf wax long-chain n-alkanes (δD_{wax}) increased from 5.6 to 0.9 ky BP suggesting a weakening in the ISM and a possible influence by the westerlies as well.

In addition, vegetation changes from pollen records, and charcoal were compared to levoglucosan/mannosan (L/M) and levoglucosan/(mannosan + galactosan) (L/(M+G)) ratios indicating that they might be a satisfactory tool to track burned fuel. The obtained results suggest that organic molecular markers are a suitable regional fire proxy and isomer ratios may help to understand changes in burned vegetation.

Acknowledgements

I would like to thank my supervisor Prof. Dr. Dario Battistel for the opportunity to write my thesis at Ca' Foscari University of Venice and for allowing me to develop this interesting research.

I would like to thank Alice Callegaro not only for supervising and helping me, but also for being a friend throughout this exciting experience in the lab. Thank you for taking the time to share your knowledge with me.

Thanks to Maria del Carmen Villoslada Hidalgo for being a friend and for helping me in the lab. Thanks to Elena Argiriadis, Elena Barbaro, Torben Kirchgeorg and everyone in the lab who has given me the scientific guidance to reach the goals in my research.

I am grateful to my Italian friends who have been helping me with the challenging but lovely Italian style, mainly during the first months. Thanks for all your support and kindness, which made this new start easier and unique. Thanks to my friends Rafa, Bia, Anca, Sara and Ceci for making bad days become better ones.

A special mention to Mattia and Giovanni. I am a better man after knowing you. I will never forget what you have been doing so far.

And finally, last but by no means least, also to Deoclides and Patricia, who made me the person I am today. Thank you for all your love and support, even if you are so far away from me. Thanks to my brothers and family. I love you and miss you very much.

Table of Contents

List of Figures

List of Tables

1 INTRODUCTION

1.1 FIRE HISTORY

In the Earth system, fire plays a critical role in ecosystem processes, such as composition and distribution of fauna and flora. Owing to strong ecological and evolutionary consequences for biota, it is impossible to understand the world without considering fire, but for a long time, the scientific community had ignored it. Evidences from the beginning of the Paleozoic Era (540 million years ago [Mya]) show that the arrival of photosynthetic organisms created an efficient environment to support combustion, albeit wildfires began soon after the arrival of terrestrial plants in the Silurian (420 Mya). Therefore, it is possible to infer that fire origin is extremely related to the first records of terrestrial plants, which contribute to two of the three essential elements to ignite it: oxygen and fuel. Heat source, through volcanic activities, meteorites and mainly through lightning, is the third missing element that has probably been available. Fig. 1 represents the necessary conditions that need to be present so that fire can happen. In spite of plenty primary productivity is required to disseminate fire, there must be a dry season that converts potential fuels into available ones. Such seasonal climates could be manifested as annual to decadal cycles of drying conditions and may arise from different weather conditions. Hence, wildfires will be powerfully managed by fuel structure and ignition frequency (Bowman et al., 2009; Pausas & Keeley, 2009; Schüpbach et al., 2015; Zhou et al., 2007).

Since the Silurian (420 Mya), fluctuations of high and low fire activity marked the evolutionary importance of fire on Earth (Fig. 2) with few evidences of charcoal in the Devonian period (400 Mya) and extensive ones in the late Paleozoic Era (345 Mya), suggesting a boost in atmospheric oxygen from the late Devonian to the late Carboniferous (Falcon-Lang, 2000; Glasspool, Edwards, & Axe, 2006; Scott, 2000). Thanks to a fall in atmospheric oxygen levels, such oscillations are proved by few evidences of charcoal deposits during the Permian (299 Mya) and the Triassic (251 Mya) periods, followed by an increase in fire wildfires in the Mesozoic Era (Jurassic and Cretaceous periods) (Pausas & Keeley, 2009; Scott, 2000).

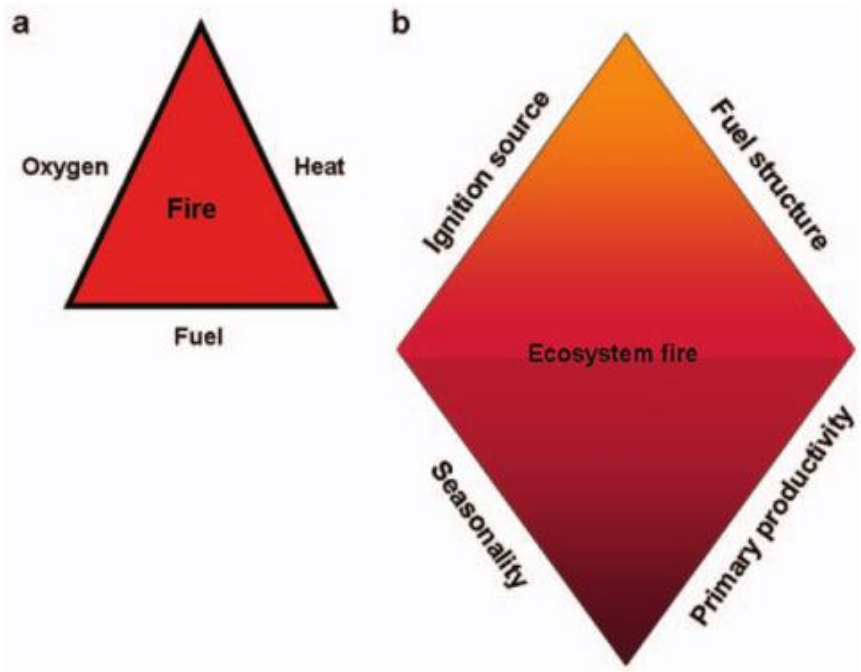

Fig. 1: Schematic of factors for (a) the physical process of fire and (b) fire as an ecosystem process (Pausas & Keeley, 2009).

During the Cenozoic Era, records indicate a global high fire activity in the Paleocene (65 Mya), followed by an abrupt decline in the Eocene (55Mya) and low activity toward the present (Bond, 2015; Diessel, 2010; Ian J. Glasspool & Scott, 2010)(Fig. 3). Shearer, Moore, & Demchuk, 1995 suggest that due to a shift from gymnosperm to angiosperm, which has much higher lignin content, coal properties completely changed in the Cenozoic, passing from a poor to a rich fossil content record of fire. During the Holocene, fire activity showed a long-term increase at global scale. Focusing on Asian continental records, the early Holocene fire activity was relatively high, followed by a lower rate in mid-Holocene, and then it has increased consistently close to late-Holocene (Bond, 2015; Miao et al., 2016; Marlon et al., 2013).

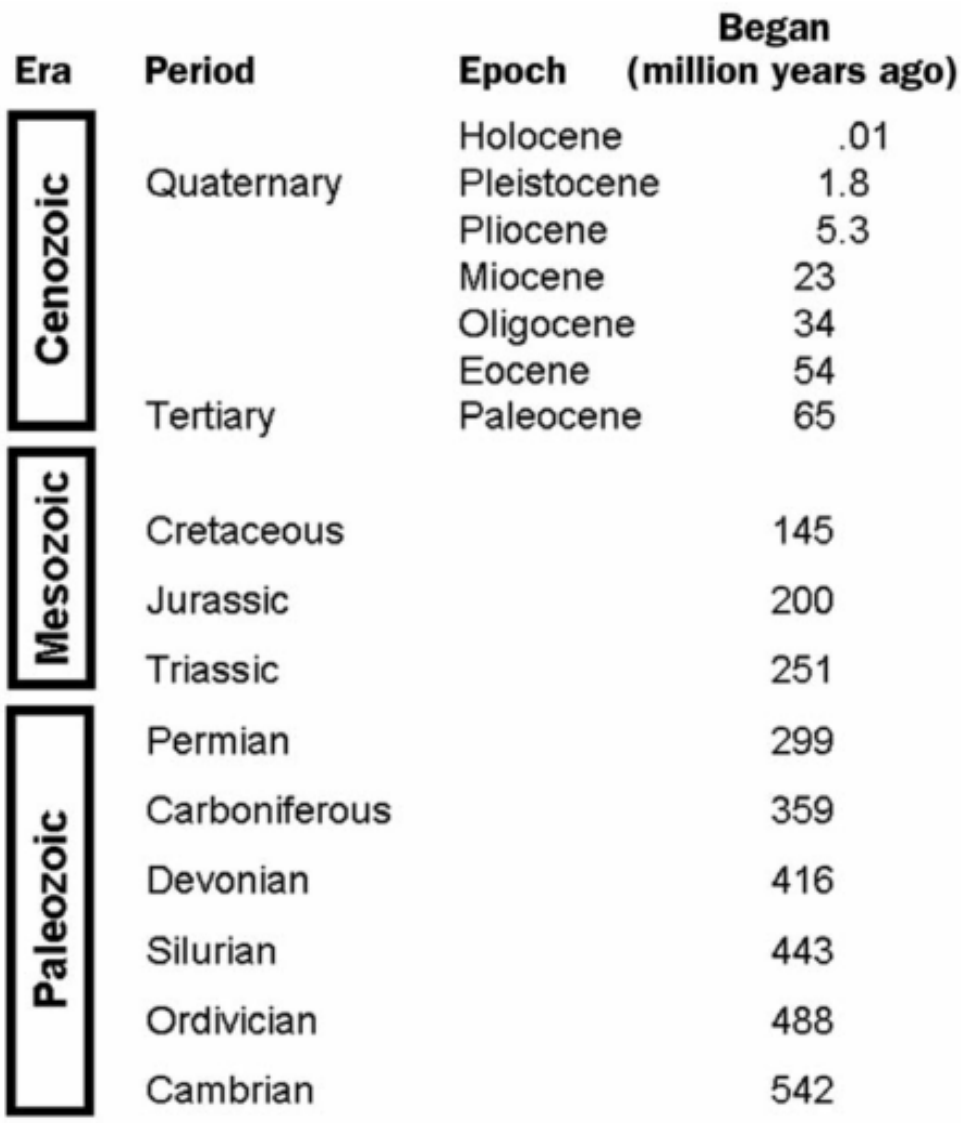

Era	Period	Epoch	Began (million years ago)
Cenozoic	Quaternary	Holocene	.01
		Pleistocene	1.8
	Tertiary	Pliocene	5.3
		Miocene	23
		Oligocene	34
		Eocene	54
		Paleocene	65
Mesozoic	Cretaceous		145
	Jurassic		200
	Triassic		251
Paleozoic	Permian		299
	Carboniferous		359
	Devonian		416
	Silurian		443
	Ordivician		488
	Cambrian		542

Fig. 2: Geological timescale (Pausas & Keeley, 2009).

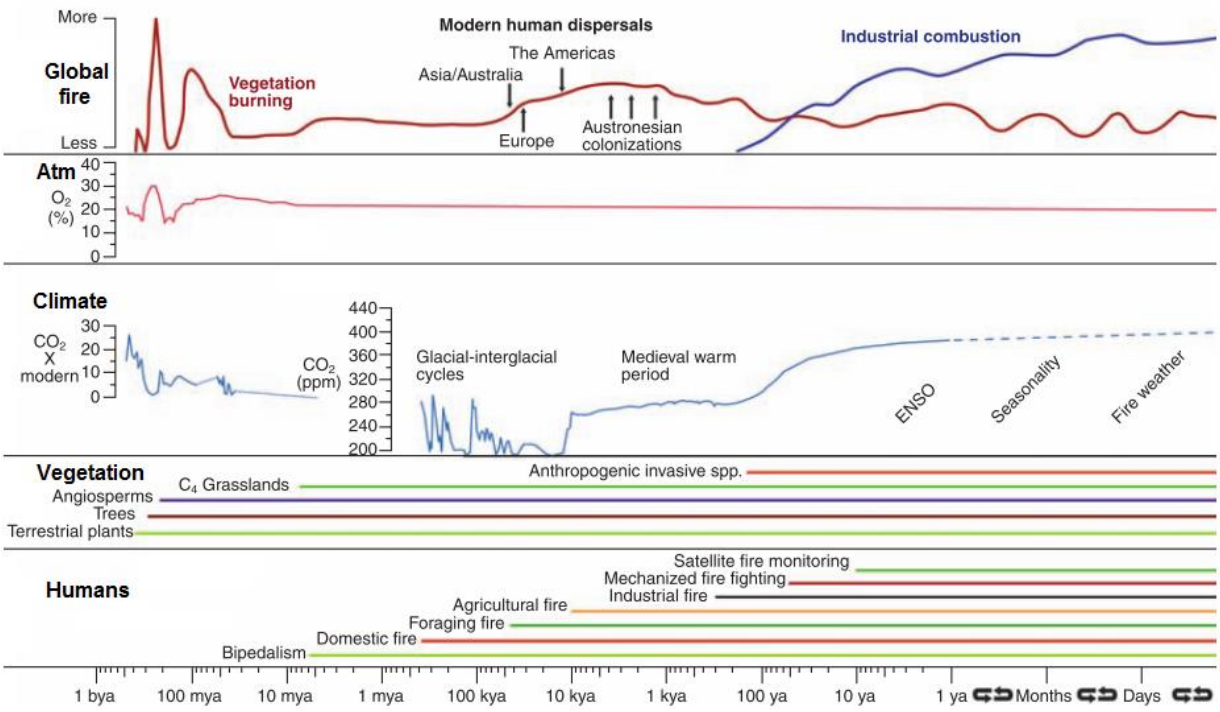

Fig. 3: Qualitative schematic of global fire activity through time, based on pre-Quaternary distribution of charcoal, Quaternary and Holocene charcoal records, and modern satellite observations, in relation to the percentage of atmospheric O_2 content, parts per million (ppm) of CO_2, appearance of certain vegetation types, and the presence of the genus Homo. Dotted lines indicate periods of uncertainty. Adapted from Bowman et al., 2009.

1.2 BIOMASS BURNING PROCESSES

Cole, 2001, states that *"biomass burning is the burning of living and dead vegetation. It includes the human-initiated burning of vegetation for land clearing and land-use change as well as natural, lightning-induced fires"*. Burning of biomass fuels has always been a natural process on Earth, proved by charcoal evidences in sedimentary records (Simoneit, 2002). Biomass is divided in four main categories (Table 1) and its different structures and compositions may vary in property, size, initial moisture content, etc (Hiltunen, Barišić, & Zabetta, 2008; Northupet al., 2005; Patel & Gami, 2012).

Cellulose, hemicellulose, and lignin are the three main polymeric components of biomass, and they approximately represent 40–60, 20–40 and 10–25 wt.% for lignocellulosic biomass (Mckendry, 2002; Yang et al., 2006) (Fig. 4). Cellulose degradation starts between 240-350 °C owing to its high resistance to thermal depolymerisation, while hemicellulose is a complex carbohydrate polymer whose thermal degradation occurs between 30–260 °C. Lignin is an unstructured and highly branched polymer that fills in the gaps left between cellulose, hemicellulose, and pectin components. It is considerably hydrophobic, decomposes between 280-500 °C and is difficult to dehydrate, thus it converts to more char than cellulose or hemicellulose (Verma et al., 2017; Yang et al., 2007).

The molecular alteration and transformation of the organic compounds emitted from biomass fuels can be influenced by the moisture, aeration, varying temperature, and duration of smouldering and flaming conditions during combustion, providing a chemical fingerprint which is source specific and useful for identifying single or multiple vegetation species (Schüpbach et al., 2015; Simoneit, 2002).

Paleofire history is a valuable source that can provide enlightenment about fire, which is sensitive to climate changes and has great impact on global biogeochemical cycles and ecosystems (Zhou et al., 2007). During dry periods, tropical grasses produce enormous amounts of highly flammable fuels, and their C4 photosynthetic pathway produces organic matter characteristically depleted in ^{13}C (Bowman et al., 2009). The amount of this stable isotope found in sediments represents that tropical savanna biomes spread in Asia, Africa, and

the Americas, matching with a spike of charcoal in marine sediments, approximately 6-8 Mya (Bowman et al., 2009; Cerling et al., 1997; Marlon et al., 2013). Thus, this finding tell us that fire led to the expansion of savannas due to hotter and drier conditions that favoured savannas (Bowman et al., 2009).

Table 1: Classification of biomass. Adapted from Patel & Gami, 2012.

Woody Biomass	Non-Woody Biomass	Process Waste	Processed Fuel
Bushes like coffee and tea	Energy crop like sugarcane	Cereal husks and cobs	Charcoal (wood & residues)
Shrubs & scrub	Soft stem (pulses and potatoes)	Bagasse (pineapple and other fruits)	Briquette/dense biomass
Tree	Grass	Plant oil cake	Biogas
Sweepings from forest floor	Bananas, plantains etc	Saw mill waste	Plant oil from palm, rape, sunflower, etc
Bamboo	Cereal straw	Municipal waste	Producer gas
Palms	Swamps and water plants	Industrial wood/ logging wastes	Methanol/ethanol (wood alcohol)

Paleofire research is pivotal because besides the large influence on environment, biomass burning can also significantly impact the global climate by releasing tropospheric particulate matter. In order to reconstruct past fire events from archaic sediments and soils, there are several suitable tracers, such as charcoal, monosaccharide anhydrides (MAs), polycyclic aromatic hydrocarbons (PAHs), and so on (Simoneit, 2002).

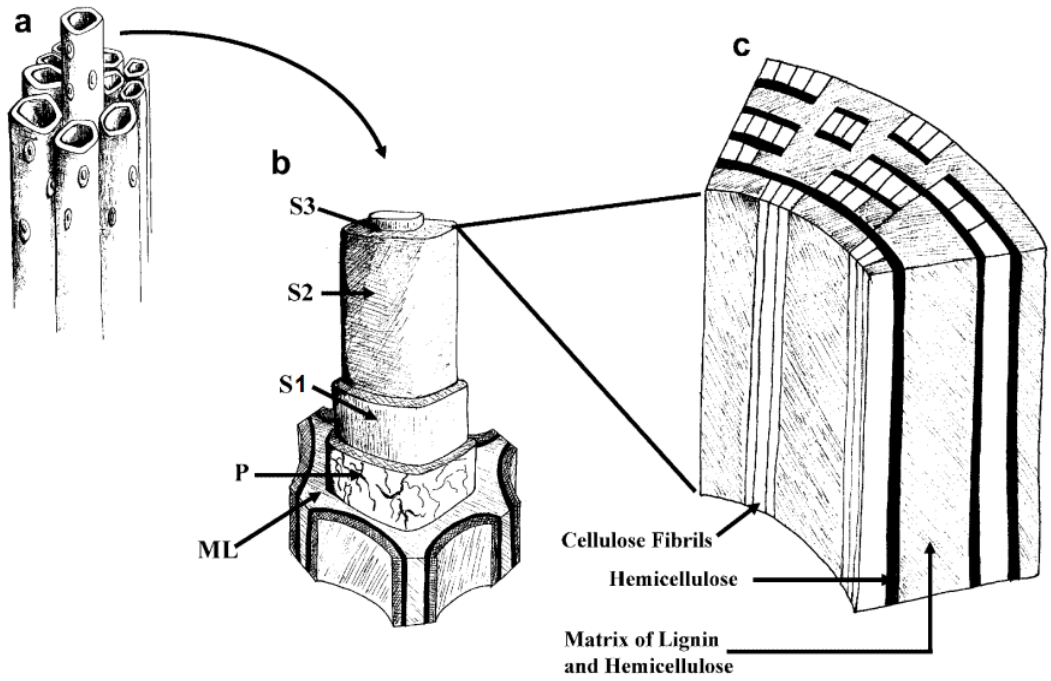

Fig. 4: Configuration of wood tissues. a) Adjacent cells; b) cell wall layers S1, S2, S3, P (primary wall), ML middle lamella; c) distribution of lignin, hemicellulose and cellulose in the secondary wall(Perez et al., 2002).

1.3 FIRE PROXIES

1.3.1 Charcoal

Charcoal is a carbon-rich solid residue formed by the pyrolysis of wood or coal, between 250° and 550°C, in the absence or limited presence of oxygen (Whitlock & Larsen, 2001). Charcoal records derived from samples of lake sediments can provide information about the range of variability in prehistoric fire regimes owing to its resistance against degradation and persistence in sediment records over millennia, making it suitable as a proxy for biomass burning (Lynch, Hotchkiss, & Calcote, 2011; Torben Kirchgeorg, 2015). However, the distance between the fire and the lake, wind direction and precipitation following the fire, other processes related to charcoal transportation, size and deposition complicate a direct fire-charcoal relationship (Fig. 5) (Whitlock & Larsen, 2001).

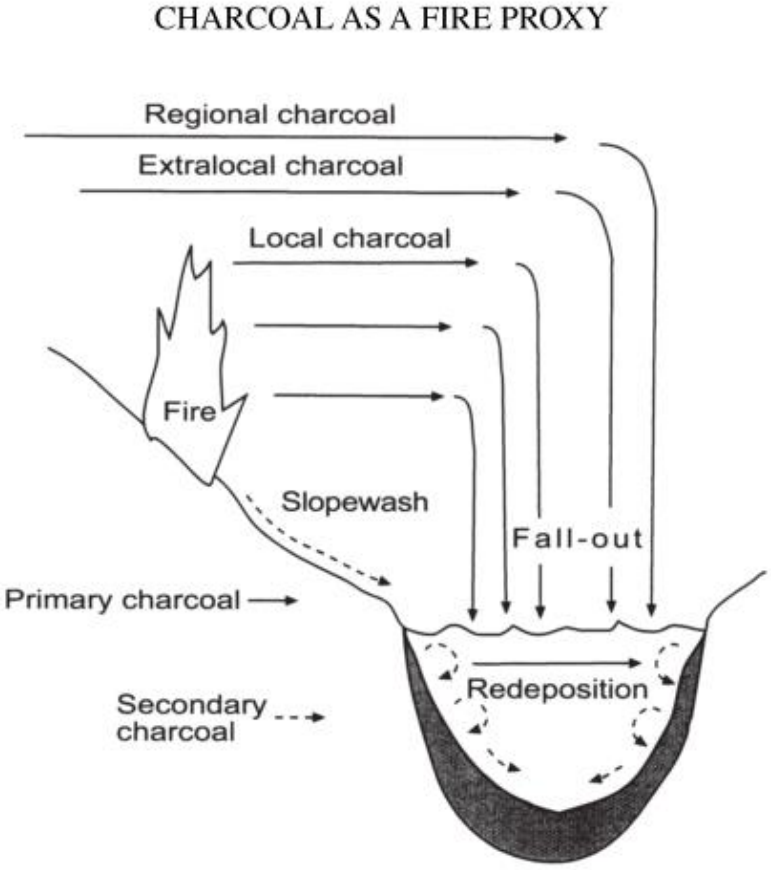

Fig. 5: Sources of primary and secondary charcoal in a watershed(Whitlock & Larsen, 2001).

Depending on its size, microscopic charcoal can be originated from distant sources, while the macroscopic one is assumed to represent local fire. Particles <100 µm in size travel well beyond 100 m, and very small ones are carried away to great heights and long distances. In principle, few charcoal particles smaller than 200µm in diameter should be deposited within 6 km of the convection column (Fig. 6). In addition, primary charcoal refers to the material introduced during or shortly after a fire event, while secondary charcoal, during non-fire years, as a result of surface run-off and lake-sediment mixing (Kirchgeorg, 2015; Whitlock & Larsen, 2001).

Enache & Cumming, 2006, suggest that many researchers agree that the temperature reached during the pyrolysis of different types of vegetation produces different types of charcoal with different densities, particle sizes,

structures, and morphologies. The moisture content of the vegetation also influences the chemical restructuring and shrinkage of the char(Bryden & Hagge, 2003). Such observations suggest that information about fire types might be deduced through careful observation of charcoal morphology and structure preserved in lake sediments (Enache & Cumming, 2006).

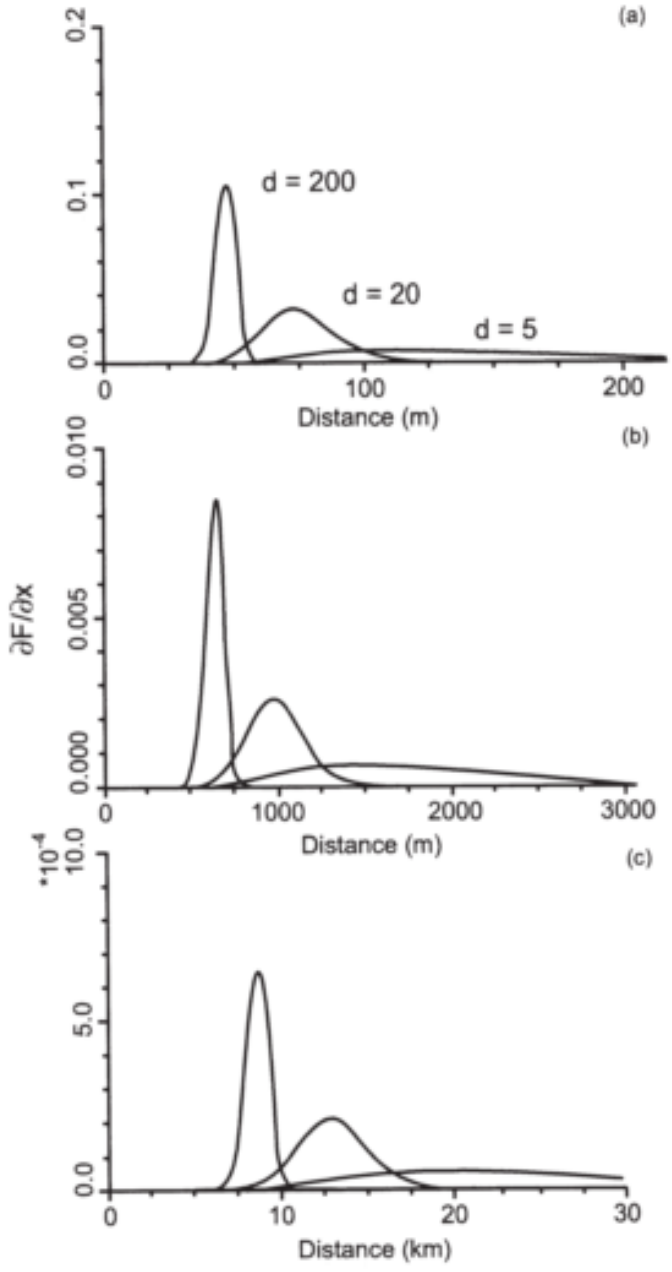

Fig. 6: Relationship between distance from the base of a fire's convective column and the amount of charcoal deposited as determined by theoretical models for charcoal particles with diameters of 200, 20 and 5 µm and convective columns with a height of (a) 10 m, (b) 100 m, and (c) 1000 m (Whitlock & Larsen, 2001).

1.3.2 Monosaccharide anhydrides

Monosaccharide anhydrides (MAs) are the greatest organic components of smoke particles released by biomass burning. Levoglucosan (1,6-anhydro-β-glucopyranose) is released when carbohydrates, such as starch and cellulose, are maximally combusted in a temperature ranging from 200 to 250 °C (Kuo et al., 2011). Owing to its relatively high stability, and its specificity to cellulose-containing substances, levoglucosan is considered a very good tracer for biomass burning. The isomers mannosan (1,6-anhydro-β-D-mannopyranose) and galactosan (1,6-anhydro-β-D-galactopyranose) are produced from hemicellulose pyrolysis (Fig. 7) (Cordell, White, & Monks, 2014; Hopmanset al., 2013; Lakshmanan & Hoelscher, 1970).

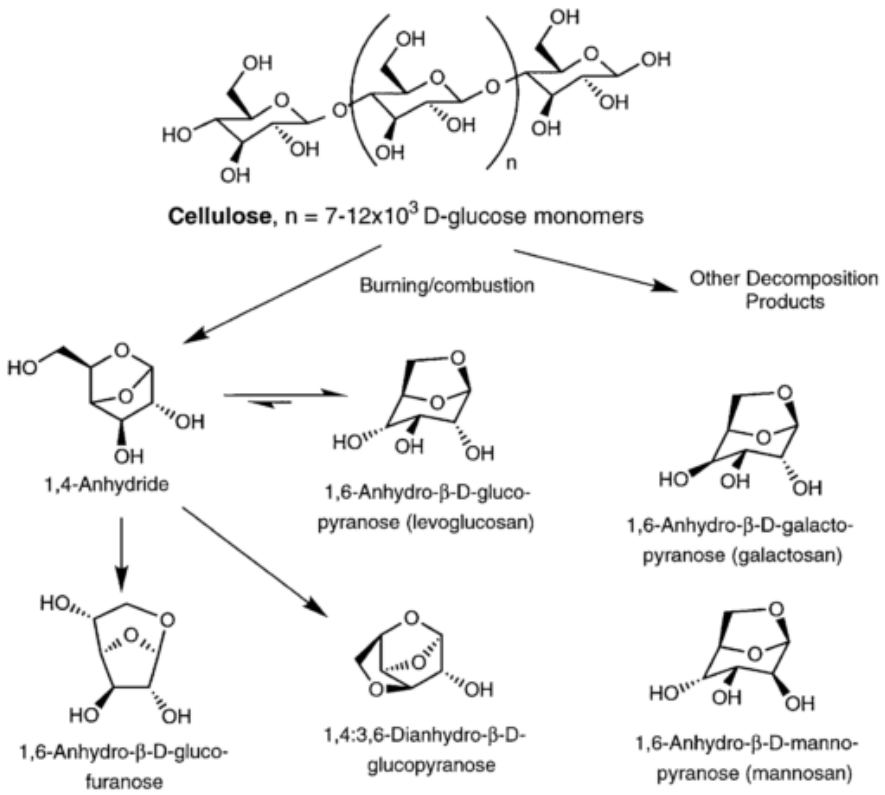

Fig. 7: The major decomposition products from burning of cellulose (Simoneit, 2002).

The ratios of these three isomers can also provide valuable information about the fire intensity, type of biomass that has been burnt, and some other

environmental conditions (You et al., 2014). Notwithstanding, Kuo, Louchouarn, & Herbert, 2011 affirmed that levoglucosan, mannosan and galactosan concentrations may vary as a consequence of the combustion temperature and duration, and the type of fuel (grass, softwood hardwood, etc).

1.3.3 Polycyclic aromatic hydrocarbons

Polycyclic aromatic hydrocarbons (PAHs) are a class of compounds made up of two or more benzene rings combined together in a linear, angular, or clustered arrangement (Fig. 8) (Zakir Hossain, Sampei, & Roser, 2013).They can be from either natural (forest and brush fires) or anthropogenic combustion sources (automobile emissions and cigarette smoke) formed both during biological processes and as products of incomplete combustion (Abdel-Shafy & Mansour, 2015). Man-made combustion sources include emissions from use of fossil fuels, while natural sources include coals, forest fires and post-depositional transformation of biogenic precursors (Zakir Hossain et al., 2013). Thus, PAHs are commonly detected in soil, air, and water (Abdel-Shafy & Mansour, 2015).

PAHs are divided in three major sources: pyrogenic, petrogenic, and biological. The first one is formed whenever organic substances are exposed to high temperatures, from 350 °C to 1200 °C, under low oxygen or no oxygen conditions, e.g. the incomplete combustion of wood in forest fires. In addition, PAHs can also be formed at lower temperatures. It is worth mentioning that crude oils contain PAHs that formed over millions of years at temperatures as low as 100–150 °C. Considering the last information, PAHs formed during crude oil maturation and similar processes are called petrogenic, e.g. oceanic and freshwater oil spills, underground and above ground storage tank leaks, and the accumulation of vast numbers of small releases of gasoline, and related substances associated with transportation. It is well-known that PAHs can be formed during the incomplete combustion of organic substances as well as in petroleum products. On the other hand, they can be synthesized by certain plants and bacteria or formed during the degradation of vegetative matter (Abdel-Shafy & Mansour, 2015; Pampanin & Sydnes, 2013; Stogiannidis & Laane, 2013). Retene, for example, can be produced in soils and sediments from the anaerobic

microbial degradation of dehydroabietic acids, defence metabolites abundant in resin, used as biomarkers for conifer plants and also produced by members of several genera of cyanobacteria (Costa et al., 2016; Stogiannidis & Laane, 2013). The isolation of PAHs directly from plant material have helped to keep alive the uncertainty of PAH biosynthesis in plants, which was assumed for a long time being formed only by pyrolysis of organic material (National Research Council (US) Committee on Pyrene and Selected Analogues, 1983). Other examples of natural sources of PAHs formation include: volcanoes, forest and brush fires, bacterial and algal synthesis, erosion of sedimentary rocks containing petroleum hydrocarbons, petroleum seeps, and decomposition of vegetative litre fall (Abdel-Shafy & Mansour, 2015).

Sediments are highly sensitive indicators of anthropogenic and natural origins, and changes in particle size, organic matter, and depositional environment are important for discovering the transport and bioavailability of PAHs in sediment and characterising their sources. The physical-chemical association of PAHs with the sediment matrix and the absence of oxygen (that fosters biodegradation) in deeper sediment layers may result in long-term PAH stability. Precipitation plays a critical role by removing the absorbed rather than the vapour phase PAHs, and in general, during cold conditions compared to warm ones, vapour phase PAHs are more efficiently removed from the atmosphere. Therefore, it should be an enrichment of low molecular weight PAHs during cold climates and higher latitudes because snow is about two orders of magnitude more effective at removing atmospheric particles than rain (Abdel-Shafy & Mansour, 2015; Stogiannidis & Laane, 2013; Vardar, Esen, & Tasdemir, 2008).

Levoglucosan and PAHs can be found in gas and particle phases, with different particle/gas partitioning. Their atmospheric lifetimes range from 1 to 26 days (Levoglucosan; Battistel et al., 2016), from 1 to 3 h (PAHs gas phase) and from 4 to 5 days (PAHs particulate phase; Lammel et al., 2009; Stier et al., 2005). According to Denis et al., 2012, although PAHs can successfully detect recent fire events within 0.5 km, they failed in detecting known fire events occurring in a range of 1 to 2 km away from the lake site. Although similar studies have not been performed for levoglucosan in sediments yet, the monosaccharide anhydride has

been detected in polar ice dating back 10 ky BP (Zennaro et al., 2014), suggesting that levoglucosan survives long-range transports.

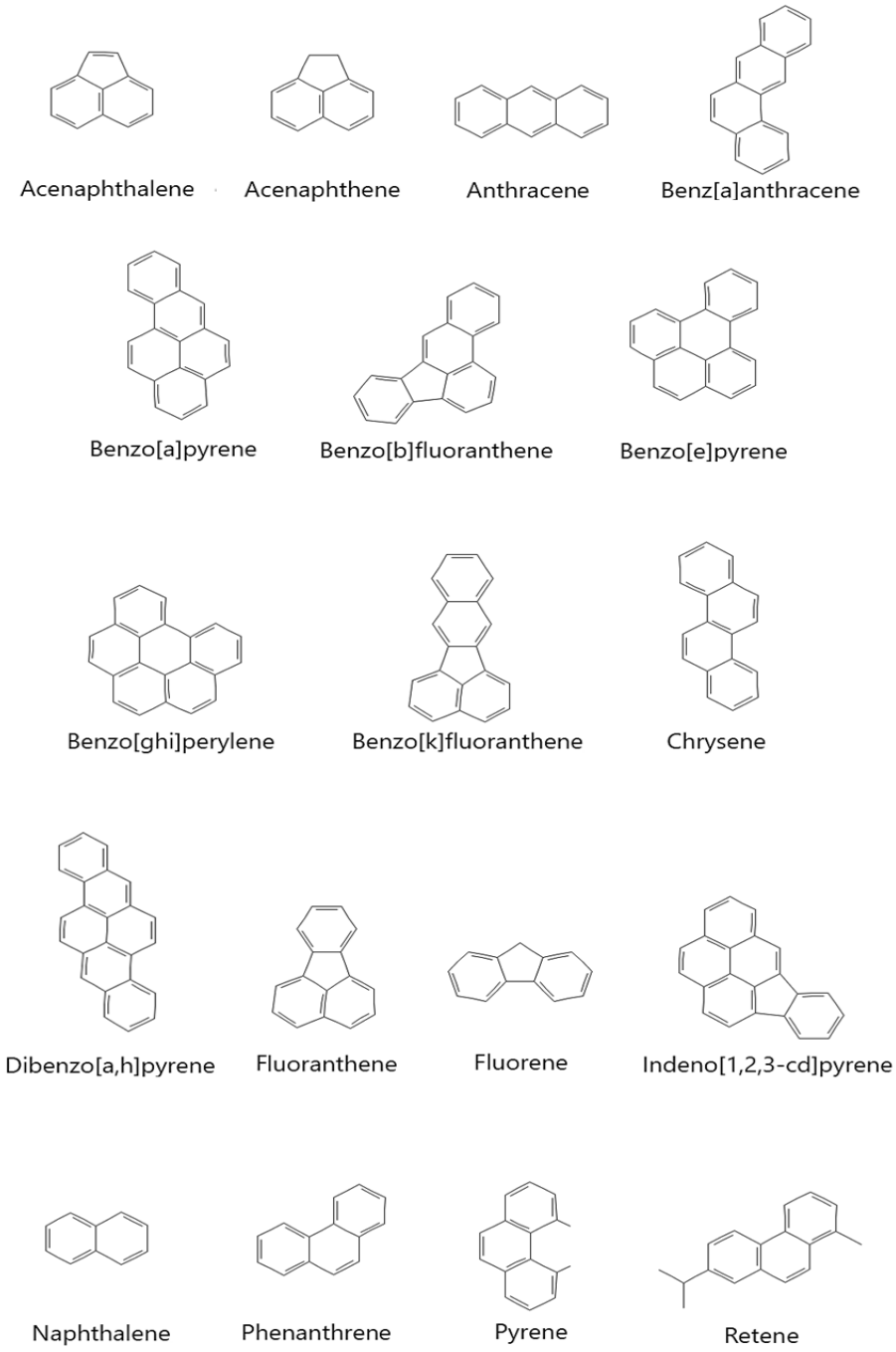

Fig. 8: The analysed polycyclic aromatic hydrocarbons (PAHs).

2 STUDY AREA

2.1 LAKE PARU CO AND THE TIBETAN PLATEAU

The Tibetan Plateau (TP) is located in Asia, which is known to be the Earth's largest and most populated continent. Its extension is approximately 1,000 km North to South and 2,500 km East to West (similar area in size to Greenland), with an average elevation exceeding 4,500 m owing to the India-Eurasia collision, altering large-scale climate systems including the Indian/Asian monsoon and westerlies, and has been suggested to have induced global cooling by erosion, chemical weathering, and declined atmospheric CO_2 (Bird et al., 2014; Heyman, 2014). In this place, the glaciers have always been the most important reservoirs of fresh water because they nourish some of the largest rivers in the world supplying water to more than 1.3 billion people, and they also contain a lot of information on the dynamics and responses of past glaciers to climate change (Dyurgerov & Meier, 2005; Xu et al., 2007). In the early 1980s, Matthias Kuhle defended his idea of an extensive glaciation with a wide ice sheet during the global last glacial maximum (LGM), ca 20 kya, rising the interest in the glacial history of the Tibetan Plateau (Heyman, 2014; Zheng & Rutter, 1998). After many repeated past glaciations, sedimentological, and geomorphological studies about the area and an intense debate subjected to harsh criticisms by other scientists, the Tibetan Plateau was marked by the glacial landforms and sediments restricted only to higher mountain areas indicating formation by alpine-style valley glaciers and icefields (Fig. 9) (Heyman, 2014; Lehmkuhl, Owen, & Derbyshire, 1998; Zheng & Rutter, 1998).

Paru Co (N29.796°, E92.352°; Fig. 10) is a small (0.1 km^2) moraine dammed lake located at 4,845 m above sea level (a.s.l.) with a maximum water depth of 1.2 m and no permanent inflows or outflows. It is hosted on the southeastern Tibetan Plateau, in the Nyainqentanglha Mountains, whose vegetation is dominated by grasses with sparse amounts of shrubs (Bird et al., 2014; Tang et al., 2000). Williams, 1983 showed that the plateau sites below 5,200 m a.s.l. have been unglaciated during the Holocene. Environmental and vegetation changes in the Tibetan Plateau have been investigated with multiple techniques, such as pollen, charcoal, MAs, PAHs records, etc (Bird et al., 2014;

Heyman, 2014; Marlon et al., 2013; Tanget al., 2000; R. Yang et al., 2016; YI et al., 2008).

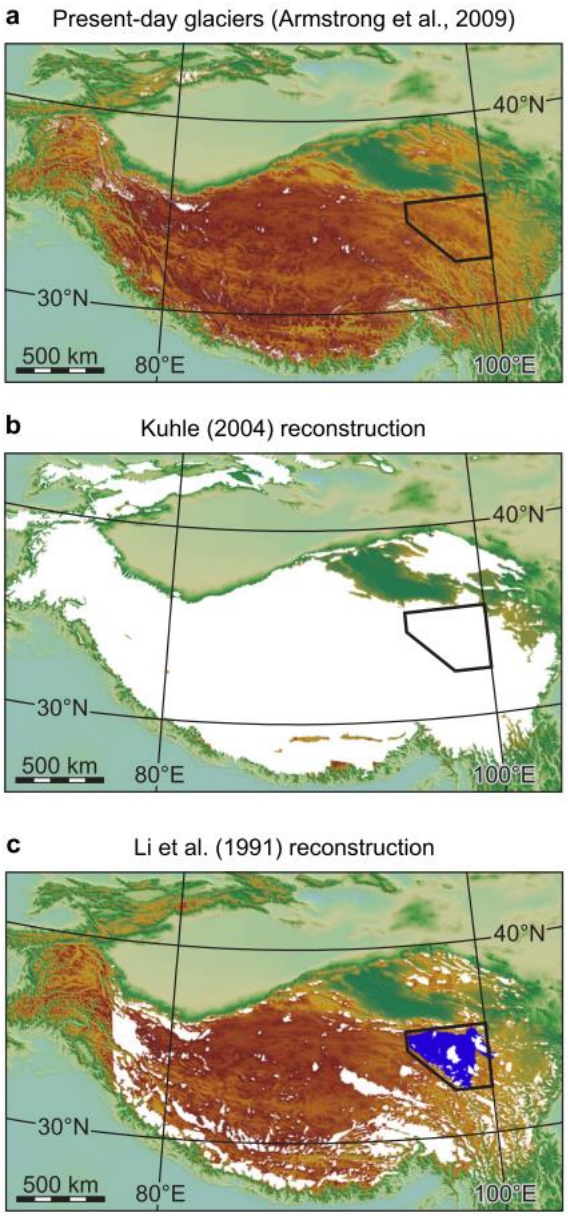

Fig. 9: The Tibetan Plateau with present-day glaciers and two paleoglaciological reconstructions. The black box marks the Bayan Har Shan study region (Fig. 2). (a) Present-day glaciers from the GLIMS project (note that not all glaciers have been mapped in the western region). (b) A plateau-wide ice sheet proposed by Kuhle (2004). (c) The glacial reconstruction from Li et al. (1991) with restricted glaciation (white) and a regional ice sheet (blue) over the Bayan Har Shan area. Adapted from Heyman, 2014.

Fig. 10: Map of southern Asia showing the location of Paru Co.

The Tibetan Plateau is affected by four climatic systems: the Westerlies, the East Indian and Asian Monsoon, and the Siberian High or Winter Monsoon (Fig. 11) (Dong et al., 2010).

Paleoclimate records show that the late Pleistocene (last glacial period) was brought to an end by an abrupt warming event at 15 kya (Severinghaus & Brook, 1999), followed by fluctuations between warm and cold conditions toward the Holocene. Records in lakes and loess deposits worldwide have proved that the early-mid Holocene were wet and warm, and high temperatures speeded up evaporation causing a shift in many lakes from open freshwater systems to saline lakes (Liu et al., 2015; Liu, Zhang, & Wan, 2009; Zhu et al., 2009). The mid-late Holocene faced a decrease in solar insolation reintroducing the cooler and drier climate at the Tibetan Plateau. (Dong et al., 2010).

Tang et al., 2000 suggest from the results of pollen records from 6 small lakes, that the evolution of South Asian Monsoon has considerably fluctuated throughout the Holocene. In 16 ky before present (BP), desert-steppe dominated the area owing to cold and dry climates, followed by an increase in temperature and precipitation which facilitated trees to live in the region after 12 ky BP. However, only between 9.2 to 6.3 ky BP, forest and forest-meadow increased in

number. After this period, the climate started to shift from warm-wet to cold-dry climate. After 5 ky BP, temperature and precipitation decreased linearly and steppe vegetation began to degenerate.

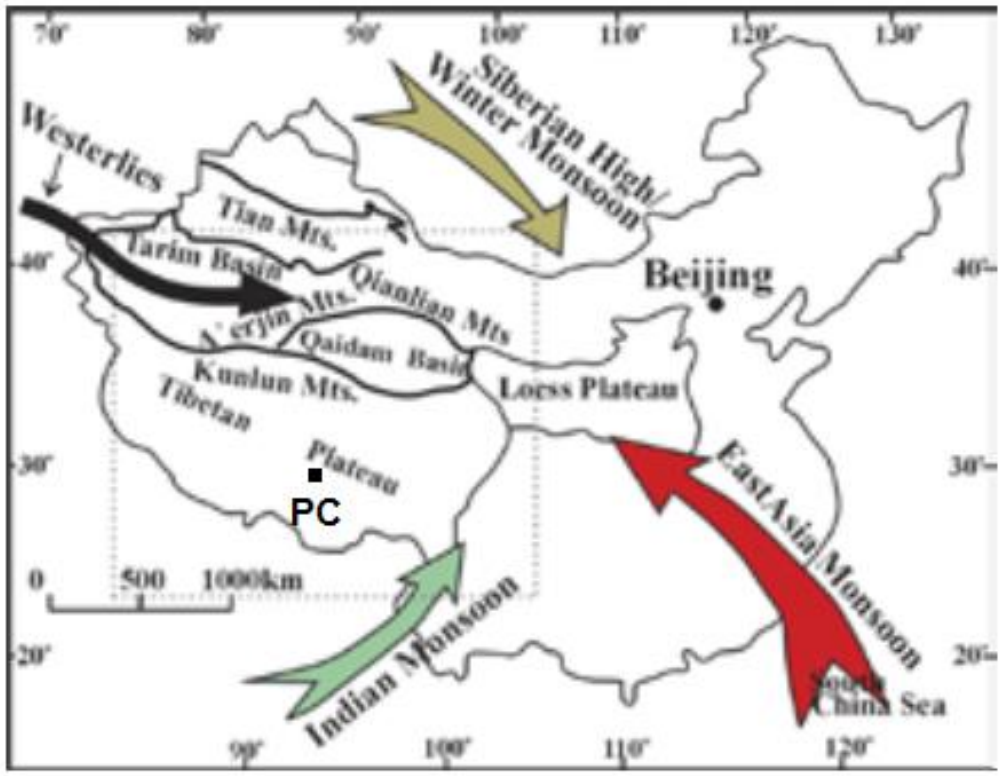

Fig. 11: Paru Co's location and major climatic systems on the Tibetan Plateau: the Westerlies, the East Asia Monsoon, the cold polar airflow from the Siberian high pressure, and the Indian Monsoon (Dong et al., 2010).

3 OBJECTIVES

Fire plays a key role in the Earth system by affecting ecosystems and climate, such as atmospheric chemistry, plants and the global carbon cycle. Understanding the role of biomass burning in the Earth system and its interactions with human activity requires examining its drivers and outcomes over temporal and spatial scales. This goal can be achieved by combining the existing paleoclimatic records with new fire reconstructions obtained in this work.

In particular, this study aims to reconstruct the paleofires history from a sedimentary record collected at Lake Paru Co, in the southeastern part of the Tibetan Plateau. Fire history will be reconstructed by determining monosaccharide anhydrides and polycyclic aromatic hydrocarbons concentration and fluxes along ~4.3 meters core section that spanned the last 11,000 years. The analysis of this record was compared with other paleoproxy sequences in order to understand fire's role in the climate of this area.

4 MATERIALS AND METHODS

4.1 SEDIMENT CORE AND AGE DEPTH MODEL

A 435 cm sediment core from Paru Co was collected in May 2011 using a modified piston corer proposed by Wright et al., 1984.The analysed core is between 55 and 435 cm deep, and was dated with the accelerator mass spectrometry (AMS) ^{14}C using six samples of carbonized grass fragments and one sample of oogonia. This core was chosen because it reasonably covers the entire Holocene, ranging from 10.9 to 1.3 ky BP. The sedimentation rate (Fig. 12) is approximately 0.35 mm y^{-1} all core length, except or the last part, between 10.9 to 10.7 ky BP, where it is ten times higher (3.3 mm y^{-1}) (Bird et al., 2014).

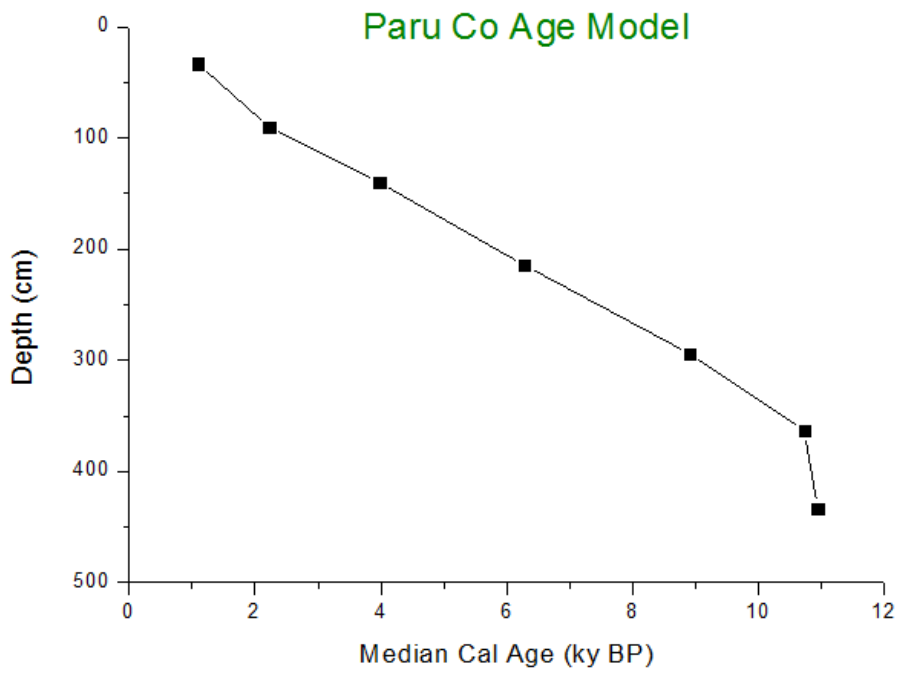

Fig. 12: Paru Co age model with AMS ^{14}C ages.

4.2 ANALYTICAL METHOD

4.2.1 Sample Preparation

72 samples were selected from the core, at 5 cm intervals, with a time resolution of approximately one hundred years. Samples were lyophilised, milled, and weighted, ranging from 0.5 to 2 grams. Then, a single extraction method, using an Accelerated Solvent Extraction (ASE Dionex-ASE 350, Thermo Fisher Scientific) with dichloromethane:methanol (DCM:MeOH) mixture (9:1, v:v), was used to extract the polycyclic aromatic hydrocarbons and monosaccharide anhydrides. In each steel ASE cell (22 mL total volume) were added a cellulose filter, diatomaceous earth, the sample, 100 µL of levoglucosan ^{13}C labelled internal standard at 1 ppm of concentration, 100 µL of a mixture of PAHs ^{13}C labelled internal standard (Acenaphthylene, Phenanthrene and Benzo[a]pyrene) at 1 ppm concentration, Na_2SO_4 in order to remove residual water and active copper in order to remove sulphur, interferent with PAHs analysis because of his similar molecular mass. The extractions were performed with three cycles of static, at 100°C of temperature, 1000 psi of pressure, and a rinse volume of 60% for every cycle. The obtained eluates were evaporated in a 200 mL glassware up to 500 µL, under a stream of N_2, using the Turbovap (Biotage, Uppsala, Sweden), in order to concentrate the samples before the clean-up. Solid-Phase Extraction (SPE) tubes containing silica gel (Supelco discovery SPE DSC-Si silica tube 12 mL, 2 g) were used to purify the two fraction samples for the analyses in gas chromatography – mass spectrometry (GC-MS) and in ion chromatography – mass spectrometry (IC-MS). A spoon of aluminium sulphate was added in order to remove particulates that can obtrude the columns of the instruments. The conditioning of the cartridges was done by using dichloromethane:hexane (DCM:Hex) mixture (1:9, v:v), then 500 µL of sample was added inside the conditioned cartridge, followed by the washing up with 40 mL of the DCM:Hex 1:9. After this process, the second fraction was collected by adding 22 mL of MeOH, in order to collect the MAs. Fraction 1 (PAHs) was evaporated under a stream of N_2, up to 150 µL in the Turbovap, at 25 °C, then analysed in GC-MS, while fraction 2 (MAs) was dried up under a stream of N_2 in the Turbovap, at 33 °C, then dissolved in 500 µL of ultrapure water under 10’ in sonic bath and

centrifuged for 5 minutes at 14,000 rpm. The supernatant was transferred to the measurement vial and then analysed in IC-MS. A blank was extracted for every batch of 10 samples.

Paru Co samples were randomly analysed in order to avoid any trend in the data that could be influenced by the extraction or measurement procedures.

4.2.2 Gas chromatography-mass spectrometry

The 17 priority PAHs have been separated by using an HP5-MS (5%-phenyl)-methylpolysiloxane column (Agilent; 325 °C: 60 m x 250 µm x 0.25 µm) for gas chromatography (GC) instrument (Agilent Technologies 7890A), combined with a mass selective detector (Agilent Technologies 5975C inert MSD). The total time for every analysis is 84.5 minutes. After GC separation, PAHs were detected with a selective single quadrupole mass detector (Agilent Technologies 5975C inert MSD) used in selective ion monitoring (SIM), looking at specific m/z ratios as can be seen in Fig. 13. The conditions were a splitless injection volume of 2 µL (split valve open after 1.5 min), He as a carrier gas (1 mL/min), 70 °C for 1.5 min, then 10 °C/min to 150 °C for 10 min, followed by 3 °C/min to 300 °C for 15 min, and 305 °C for 30 min (post run). Inlet and interface temperature were at 300 °C.

The MS instrument was equipped with an electronic impact (EI) source used in positive ionisation mode (70eV). The source temperature was 230 °C and the quadrupole temperature was 150 °C. Samples were quantified using response factors containing 17 studied PAHs plus labelled ^{13}C Acenaphthylene, ^{13}C Phenanthrene and ^{13}C Benzo[a]pyrene (isotope dilution method). The advantage is the ability to correct potential analyte losses during extraction and handling. The obtained values for the limit of detection (LOD) and limit of quantification (LOQ) were calculated by the mean of the blanks plus three times the standard deviation, and mean of the blanks plus ten times the standard deviation (Table 2), respectively, while the precision was around 15 % of the amount obtained for each PAH.

PAHs were separated in GC, then analysed in MS by their m/z ratios, as can be seen in Fig. 13. The stable isotope labelled internal standards ^{13}C

Acenaphthylene, ^{13}C Phenanthrene and ^{13}C Benzo[a]pyrene, with m/z 158, 184 and 256, respectively, are present to quantify the other ions in each sample.

Table 2: PAH ions, their m/z ratios, and their average retention time from a response factor.

PAHs	Abbrev	m/z	Retention time	LOD	LOQ
Naphthalene	Naph	128.1	11.55	15.96	27.18
Acenaphthylene	Acy	152.1	19.33	8.42	12.56
Acenaphthene	Ace	154.1	20.91	17.82	37.40
^{13}C Acenaphthylene	^{13}C Acy	158.1	19.32	-	-
Fluorene	Flu	166.1	25.38	8.66	17.41
Phenanthrene	Phe	178.1	33.73	21.42	27.91
Anthracene	Ant	178.1	34.13	19.25	19.25
^{13}C Phenanthrene	^{13}C Phe	184.1	33.73	-	-
Fluoranthene	Fl	202.1	43.80	11.09	14.45
Pyrene	Pyr	202.1	45.50	19.39	20.67
Benzo[a]anthracene	BaAnt	228.1	55.26	-	-
Chrysene	Chr	228.1	55.56	-	-
Retene	Ret	234.1	48.62	-	-
Benzo[b]fluoranthene	BbFl	252.1	63.23	-	-
Benzo[k]fluoranthene	BkFl	252.1	63.40	-	-
Benzo[a]pyrene	BaPyr	252.1	65.327	15.83	28.13
Benzo[e]pyrene	BePyr	252.1	66.20	-	-
^{13}C Benzo[a]pyrene	^{13}C BaPyr	256.1	65.317	5.90	5.90
Benzo[g,h,i]perylene	BghiPer	276.1	72.47	-	-
Indeno[1,2,3-c,d]pyrene	IPyr	276.1	74.13	-	-
Dibenz[a,h]anthracene	DBahAnt	278.1	72.72	-	-

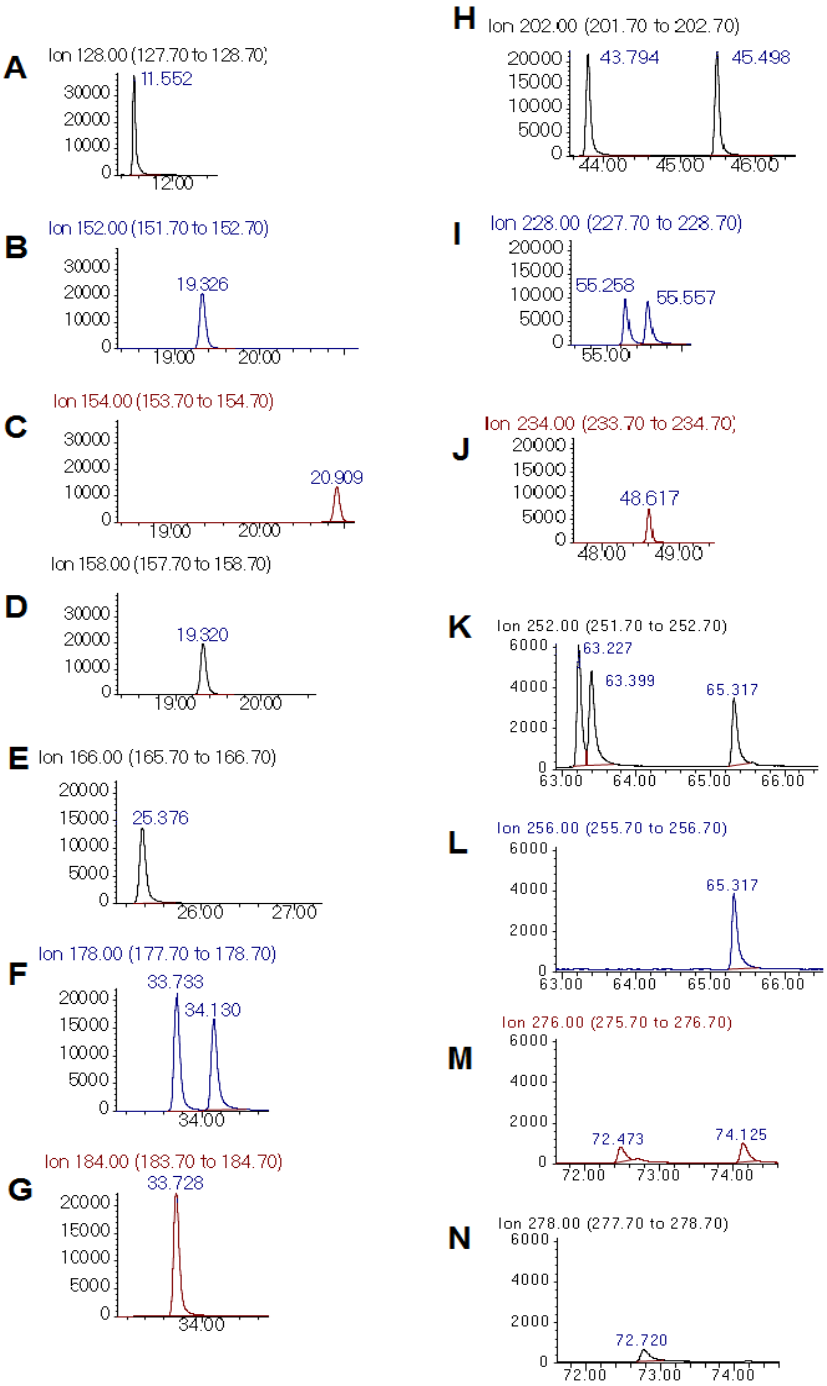

Fig. 13: PAH chromatograms with their retention times and m/z from a DCM:Hex 1:9 solution containing 100 ng μl^{-1} of; **(A)** Naphthalene; **(B)** Acenaphthylene; **(C)** Acenaphthene**; (D)** ^{13}C Acenaphthylene; **(E)** Fluorene; **(F)** Phenanthrene and Anthracene; **(G)** ^{13}C Phenanthrene; **(H)** Fluoranthene and Pyrene; **(I)** Benzo[a]anthracene and Chrysene; **(J)** Retene; **(K)** Benzo[b]fluoranthene, Benzo[k]fluoranthene and Benzo[a]pyrene; **(L)** ^{13}C Benzo[a]pyrene; **(M)** Benzo[g,h,i]perylene and Indeno[1,2,3-c,d]pyrene; **(N)** Dibenzo[a,h]anthracene.

4.2.3 Ion chromatography-mass spectrometry

Levoglucosan, mannosan and galactosan were separated by using an ion chromatography (IC) instrument (Dionex ICS 5000, Thermo Scientific, Waltham, US) combined with a CarboPac™ MA 1 and AminoTrap columns (Thermo Scientific; 2 mm x 250 mm). The retention time of these three isomers (m/z 161) is ~6.5 min, ~10 min and~16 min for levoglucosan, mannosan and galactosan, respectively, and ~6.5 min for the stable isotope labelled internal standard (m/z 167), i.e. the ^{13}C levoglucosan (Fig. 14 a-b). The three MAs were detected with a single quadrupole mass spectrometer (MSQ Plus™, Thermo Scientific) after IC separation. The injection volume was 50 µL and NaOH (flow of 250 µL /min) was produced as a carrier solvent by an eluent generator (Dionex ICS 5000 EG, Thermo Scientific). The gradient was: 20 mM (0–23 min), 100 mM (23–43 min; column cleaning), 20 mM (43–53 min; equilibration). NaOH was removed by a suppressor (ASRS 300, 2 mm, Thermo Scientific) before entering the MS source, in order to protect the instrument during the analysis. The flow was switched to waste after a total run time of 23 min. A 7 ‰ solution of MeOH/NH_4OH was added in the post column (25 µL/min) to improve the ionization of the aqueous eluent. Atmospheric N_2 was used to avoid external contamination and pressure oscillation.

The MS instrument was equipped with an electrospray ionization (ESI) source used in negative ionization mode. The source temperature was set at 350 °C, the needle voltage was -2.5 kV and the cone voltage -50 V. Samples were quantified using a calibration of response factors of natives L, M and G vs. the ^{13}C labelled internal standard levoglucosan, which is present to quantify the other ions in each sample. The obtained values for LOD is 4.5 ppb and for LOQ is 14.5 ppb, while the standard error was around 20% of the amount obtained for each MAs.

The running time for a single analysis is around 60 minutes due to the use of two columns. This is necessary to remove all residual sugars in order to avoid carryover effects, as MAs can be generated in the electrospray ionisation (ESI) source with a temperature higher than 300 ºC. Therefore, a long cleaning and reconditioning step is required after each sample injection. Fig. 14c shows a

typical chromatogram obtained in a real sample, where MAs were successfully separated.

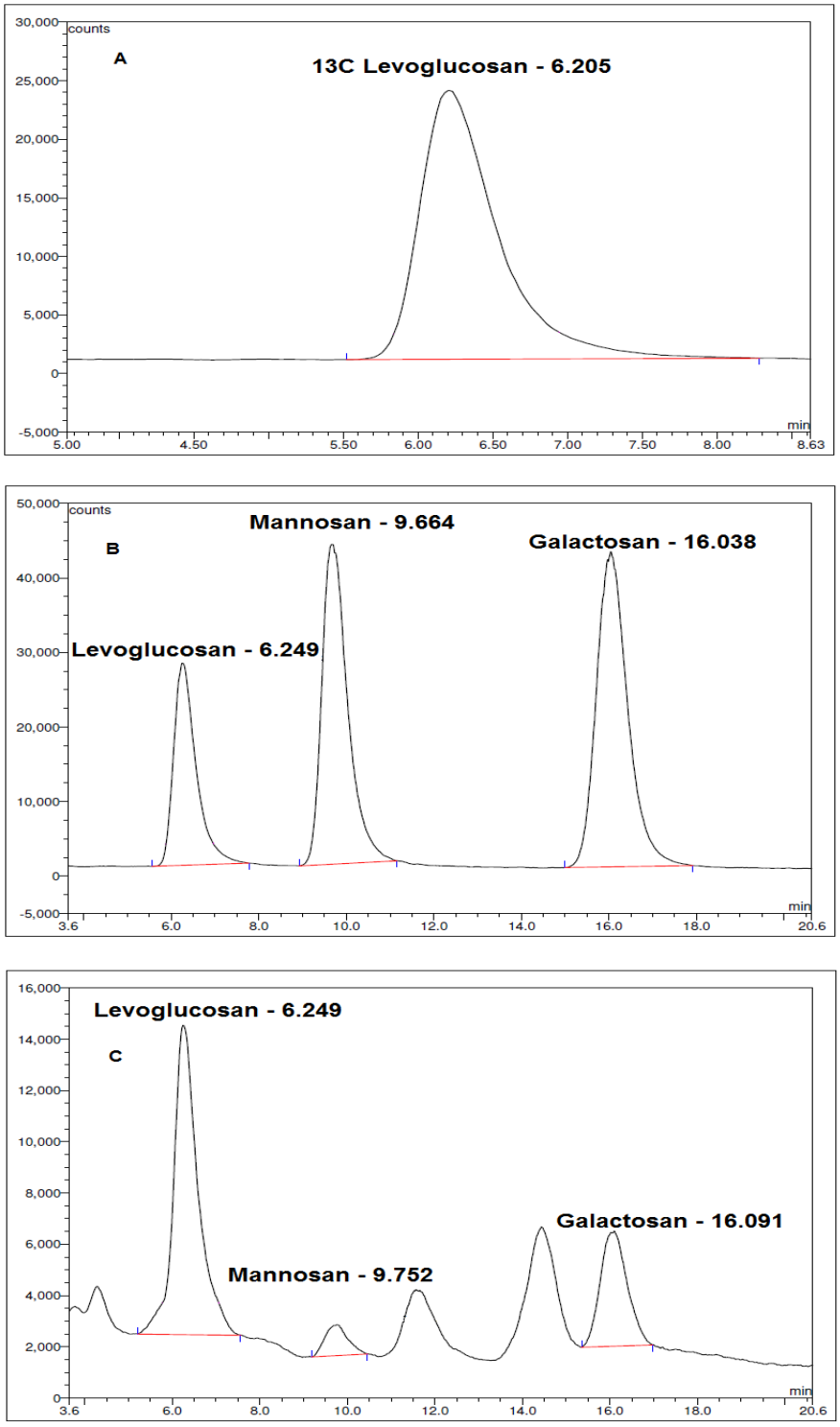

Fig. 14: Chromatogram **(a)** of the ^{13}C levoglucosan (250 ppb - m/z 167); **(b)** of a standard mixture (250 ppb - m/z 161) of levoglucosan (L), mannosan (M) and galactosan (G); **(c)** of the sample PC 3 – 65 and their retention times.

5 RESULT AND DISCUSSION

Fluxes of the monosaccharide anhydrides were calculated for each sample by multiplying sedimentation rate, wet density and concentration of the respective MAs, as illustrated in Fig. 15.

$$\text{L Flux}\left(\frac{ng}{cm^2y}\right) = \text{sedimentation rate}\left(\frac{\text{cm}}{y}\right)\text{x wet density}\left(\frac{g}{cm^3}\right)\text{X [L]}\left(\frac{ng}{g}\right)$$

$$\text{M Flux}\left(\frac{ng}{cm^2y}\right) = \text{sedimentation rate}\left(\frac{\text{cm}}{y}\right)\text{x wet density}\left(\frac{g}{cm^3}\right)\text{X [M]}\left(\frac{ng}{g}\right)$$

$$\text{G Flux}\left(\frac{ng}{cm^2y}\right) = \text{sedimentation rate}\left(\frac{\text{cm}}{y}\right)\text{x wet density}\left(\frac{g}{cm^3}\right)\text{X [}G\text{]}\left(\frac{ng}{g}\right)$$

Fig. 15: Flux equations for levoglucosan (L), mannosan (M) and galactosan (G)

The fluxes of levoglucosan, mannosan and galactosan in Paru Co samples ranged from 1-2,500, 0.5-163 and 0.6-532 ng cm^{-2} y^{-1}, respectively. An overview of the fluxes is shown in Fig. 15 and all data were blank corrected.

Fig. 16 shows the obtained levoglucosan, mannosan and galactosan fluxes. In the inset, in Fig.16, the complete record ranging from 1.3 to 11 ky BP was also reported. These two graphs for each MA were used to facilitate the comprehension of their amounts throughout the Holocene. As it can be seen from Fig. 16, the early Holocene has the highest concentrations of levoglucosan, mannosan and galactosan between 11 and 10.7 ky BP. This high MAs signal is then followed by a sharp decrease up to 7.5 ky BP. As it is shown, a long-term decreasing trend for all MAs was observed.

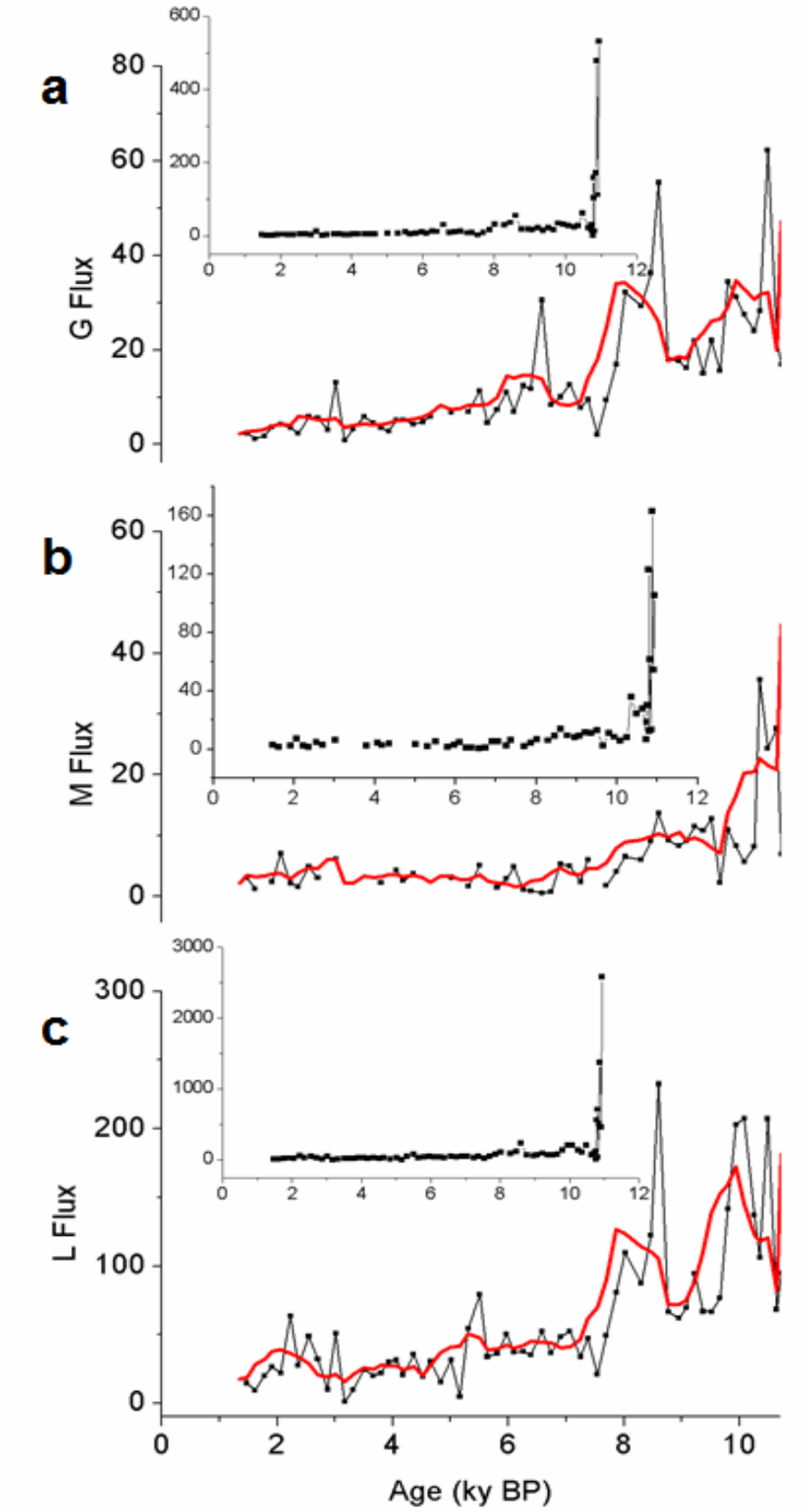

Fig. 16: Results from Paru Co are in fluxes: **(a)** galactosan; **(b)** mannosan; **(c)** levoglucosan.

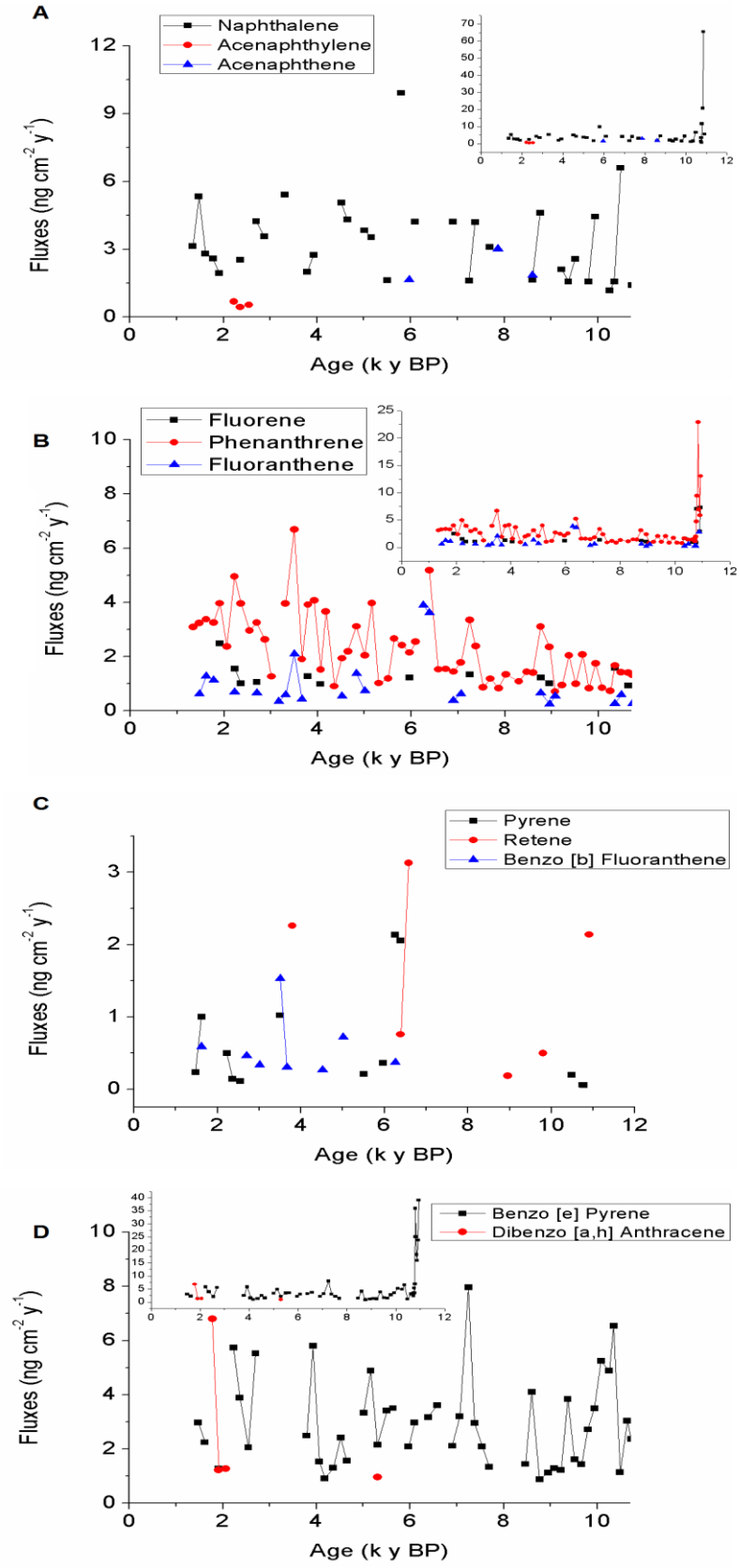

Fig. 17: Results from Paru Co in fluxes: **(A)** Naph, Acy and Ace; **(B)** Flu, Phe and Fl; **(C)** Pyr, Ret and BaFl; **(D)** BePyr and DBahAnt.

PAH fluxes were calculated in the same way as MAs fluxes (sedimentation rate x wet density x PAH concentration). and the results are shown in Fig. 17. Naphthalene, Fluorene, Fluoranthene, Phenanthrene and Benzo[e]pyrene have the highest concentrations throughout the Holocene, mainly between 10.9 and 10.7 ky BP, similarly to MAs record.

Paru Co represents a Holocene fire record ranging from 11 to 1.3 thousand years before present. According to Bird et al., 2014, Paru Co's records, based on sedimentation rate and dry bulk density (ρ_{dry}), could be divided into two periods, one from 10.9 to 10.7 ky BP and one from 10.7 ky BP to the present (Fig. 18). Elevated sedimentation rate and ρ_{dry} likely reflect glacial sedimentation during the early Holocene from 10.9 to 10.7 ky BP. After 10.7 ky BP, significant reductions in the stabilisation of sedimentation rates and ρ_{dry} suggest that glacial activity ended in the small moraine dammed lake at this time and the catchment remained unglacierised until now. Sediment deposition only occurs during the Boreal Summer when the lake is unfrozen. Therefore, after 10.7 ky BP, sedimentological variability is linked to Summer climatic conditions and variations in Indian Summer Monsoon (ISM) rainfall. Due to that, variability in Paru Co's sediment constituents are considered to reflect climatic, not glacial processes.

%Lithic and % Biogenic Silica (%BSi) have a correlation coefficient (r) of -0.97 and a coefficient of determination (r^2) of 0.95. This likely reflect a dilution and productivity effect, depending on the abundance of clastic material entering the lake and its influence on diatom productivity and water column turbidity. The anti-phased relationship between both of them shows that an increase in lithic flux was counterbalanced by a decrease in %BSi and vice versa (Fig. 18a,b). The % of total organic matter (%TOM) (Fig. 18c) showed a small variability with an increasing trend throughout the Holocene, indicating that Paru Co's depositional environment is influenced by the contribution of clastic material into the lake. The contribution of summer (90%) over winter (10%) precipitation indicates that Indian Summer Monsoon (ISM) rainfall was boosted from 10.1 to 7.1 then decreased to a minimum between 7.1 and 3.4 ky BP. It increased during the late Holocene in 3.4 and 1.9 ky BP, and decreased again after 0.3 ky BP(Bird et al., 2014).

According to Hong et al., 2003, there is a weakening of the ISM around 4.2 ky BP that possibly caused severe drought conditions which has also been observed in the widespread area besides the Hongyuan site, including the western Tibetan Plateau, the Mesopotamian plain in western Asia and the western Africa and Mexico regions, which have been considered to harshly hinder the development of ancient civilization in these areas. Consistent with the δD_{wax} record, Lake Qinghai, Seling Co and Bangong Co show increases in isotopic values after between 5 and 4 ky BP which is a coherent weakening of ISM rainfall information (Bird et al., 2014) that was also inferred by Hong et al., 2003. During boreal summer (austral winter), the sensible heating supply in land and ocean are different and leads to the seasonal formation of low atmospheric pressure over the Tibetan Plateau. Simultaneously, sea surface temperature (SST) of the southern subtropical Indian Ocean is relatively colder during the boreal summer, creating high atmospheric pressure over the southern subtropical Indian Ocean. When facing high temperatures and humidity, cross-equatorial transports of latent heat and the strong summer monsoon winds cross through the Arabian Sea and the Bay of Bengal, respectively, reaching the Tibetan Plateau. Records from Hongyuan Bog, Lake Naleng and Ximencuo support the idea of mainly having warmer and wetter ISM between ~11 and 5 ky BP, followed by a cooler and drier conditions. Paru Co results are also similar to many regional lake reconstructions, like DongiiConna, Zhari Nam Co and Ahung Co. The last one suggests maximum lake levels between 9 and 7.5 ky BP (high ISM precipitation), followed by a decreasing lake levels until ~4 ky BP when deposition in the lake basin ceased, indicating maximum clastic deposition during the early Holocene until 7.1 ky BP (Bird et al., 2014). %BSi is lower when ISM rainfall is high because it grows more biomass, which will be available to be burnt, as pointed out in Fig. 18d, when high levoglucosan was detected in 8.6 ky BP. Mischke & Zhang, 2010, based on the Lake Ximencuo records, inferred that six relatively short-lived cold periods happened about 10.3–10.0, 7.9–7.4, 5.9–5.5, 4.2–2.8, 1.7–1.3 and 0.6–0 ky BP. Most of these events are similarly recorded in the peat sections from the close lakes (Ximencuo and Hongyuan).

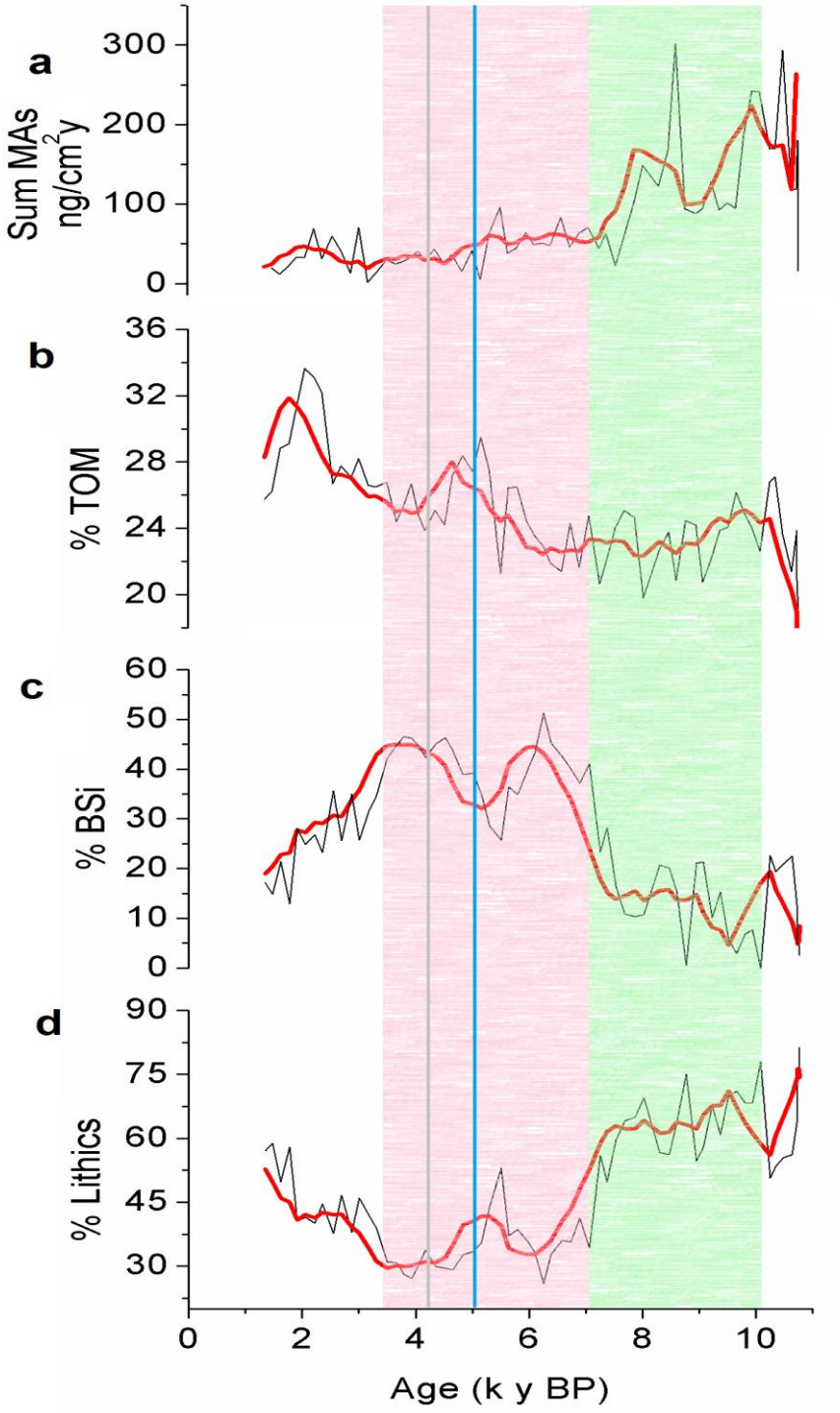

Fig. 18: Results from Paru Co showing **(a)** ∑MAs; **(b)** %TOM; **(c)** %BSi; **(d) %**lithics. Green box indicates that ISM rainfall increased from 10.1 to 7.1 ky BP. Pink box shows the decrease of ISM rainfall to a minimum between 7.1 and 3.4 ky BP. Grey line represent the weakening of the ISM around 4.2 ky BP. Blue line illustrates the division between warmer and wetter ISM between ~11 to 5 ky BP, followed by a cooler and drier conditions.

The concentrations and distributions of PAHs in sedimentary basins depend on the rate of sedimentation, as well as their source and diagenesis, with variable sediment dilution effects among river/lacustrine and marine environments. The relative proportions of PAHs derived from land areas are generally independent of sedimentation rate (Zakir Hossain et al., 2013). Therefore, the relative composition of the PAHs could record information of terrigenous/land environment in the Paru Co succession.

Fig. 19 illustrates the trends comparison between MAs, whose signal is mainly due to levoglucosan, and PAHs, which can come from a natural or anthropogenic sources.

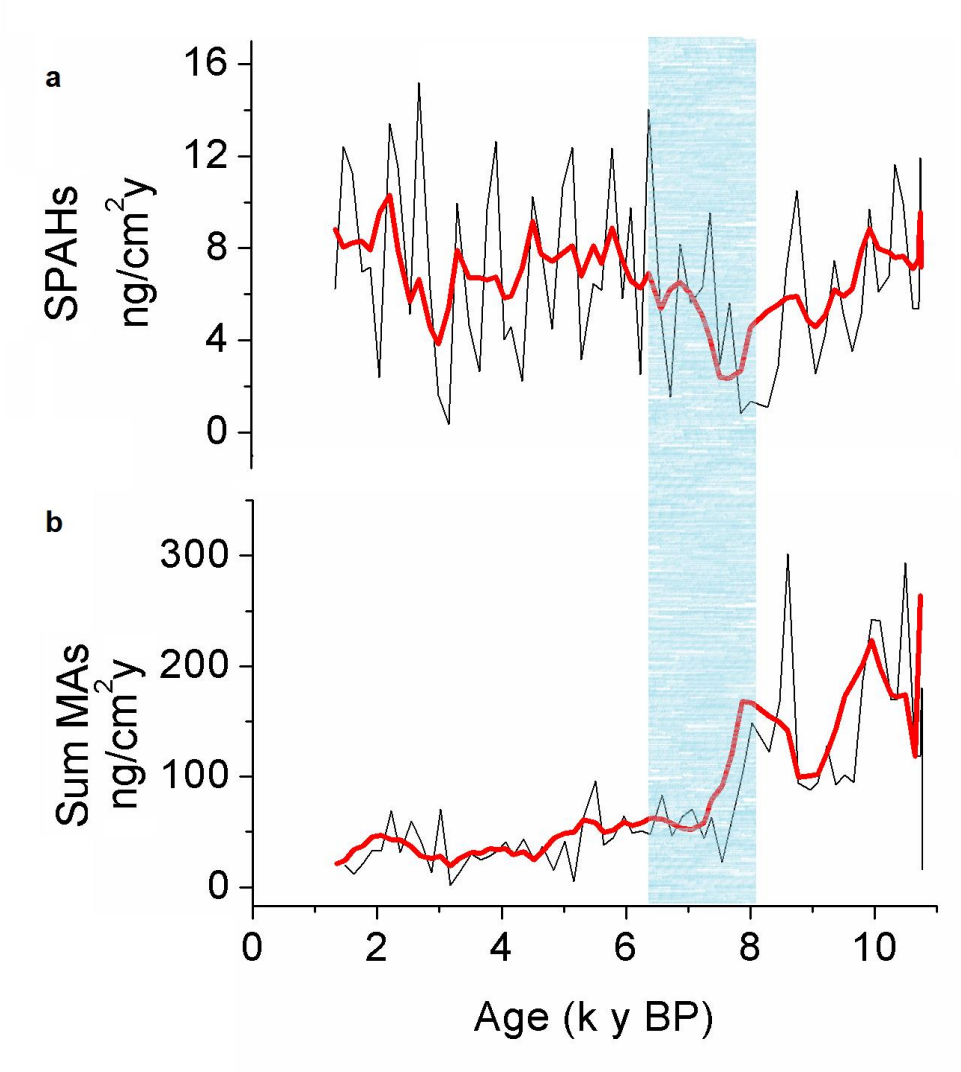

Fig. 19: Results from Paru Co showing the trends of **(a)** ∑PAHs and **(b)** ∑MAs at Paru Co.

Looking at Fig. 19, it is clear that throughout the Holocene, the sum of the obtained data for PAHs and MAs are not correlated at all (r = 0.16), and the same happened for their trends, obtained with a moving average (r = 0.30). However, paying attention only on their trends and dividing the Holocene into two parts, one from 11.0 to 8.7 ky BP (r = -0.82) and the other, after 8.7 ky BP (r = 0.69), their trends seem more correlated. Therefore, it is likely to presume that in the period 11.7-8.7 ky BP, the contributions of PAHs were a result of wildfires while after 8.7 PAHs input may have a difference source (i.e. biogenic or both biogenic and pyrogenic) In fact, according to Stogiannidis & Laane, 2013, biogenic PAHs are produced by plants, algae/phytoplankton and microorganisms, whereas diagenetic PAHs are produced during the slow transformation of organic materials in lake sediments. Diagenetic PAHs refer to biogenic precursors, like plant terpenes, leading to the formation of compounds such as derivatives of phenanthrene (Wiley & Sons, 2003). Other PAHs such as BbFl, Phe and Naph can be originated from vascular land plants or termite activity. BePyr (the second highest concentration at Paru Co) and BbFl are highly resistant to oxidation processes. BaPyr disappears in severe weathering conditions and low amounts of BaAnt and BaPyr could be also due to solubilisation or biodegradation in an oxic water column, or to prolonged exposure in an oxic bottom environmental condition. This can explain why they were not found in any sample. BghiPer (5-ring) generally has its origins in combustion (Killops and Massoud, 1992; Leeming and Maher,1992; Jiang et al., 1998), and have been reported from high intensity paleovegetation fires (Finkelstein et al., 2005; Denis et al.,2012). When fuel sources are uniform, hotter fires commonly produce elevated concentrations of 5- and 6-ring PAHs. In addition, highly pericondensed compounds, such as BePyr, are minimally susceptible to alteration and biodegradation (Zakir Hossain et al., 2013).

Table 3: sum of each PAH found in Paru Co.

PAH	∑(ngcm^{-2}y^{-1})
Naph	218.82
Acy	1.67
Ace	6.53
Flu	35.90
Phe	223.87
Fl	24.99
Pyr	8.09
Ret	17.80
BbFl	4.59
BePyr	331.80
DBahAnt	10.27

As can be seen in Table 3, the highest concentrations throughout the Holocene at Paru Co are BePyr, Phe and Naph.

Levoglucosan, mannosan and galactosan are emitted in varying ratios because they depend on the burning conditions, vegetation type and temperature (Kirchgeorg, 2015). The ratios between levoglucosan/mannosan (L/M) and levoglucosan/(mannosan + galactosan) (L/(M+G)) may track changes in past burnt fuels, but the major problem to asses them is that the broad ranges of MA ratio values from different papers overlap, limiting the conclusions about the burnt biomass (Engling et al., 2006; Fabbri et al., 2009; Kirchgeorg et al., 2014; Kirchgeorg, 2015; Kourtchev et al., 2011; Kuo, Louchouarn, & Herbert, 2011; Schüpbach et al., 2015) (Table 4).

According to Kuo et al., 2011, after 5 h of prolonged combustion at constant temperature (250 °C), mannosan and galactosan levels continuously decreased, compared to the results obtained after 0.5 h combustion, while levoglucosan presented no significant change. Higher combustion temperature (300 °C) and

longer combustion duration result in higher ratios, regardless of plant species. This happens because mannosan and galactosan derive from the combustion of hemicellulose, which have a higher thermal lability, i.e. they can be changed or destroyed at high temperatures, compared to that of levoglucosan, a cellulose combustion by-product, which may explain such overlapping data (Simoneit, 2002; H. Yang et al., 2007). Therefore, under such circumstances, the power of the anhydrosugar ratios for source discrimination is seriously weakened and more complex parameters should be taken into consideration in order to better interpret these results.

Table 4: Ratios of anhydrosaccharides in source test emissions from lignite and biomass burning. Adapted from Fabbri et al.(2009).

Biomass type	L/M	L/(M+G)	Data source
Lignite Jsp11	31-92	31-92	Fabbri et al. (2009)
Hardwoods	22	17.6	Nolte et al. (2001); Fine et al. (2002)
	13-24	-	Fine et al. (2004)
	14.5-14.6	8.5-9.9	Schmidl et al. (2008)
	13.8-32.3	4.4-15	Engling et al. (2006), Kuo et al. (2001a)
Softwoods	4	3.6	Nolte et al. (2001); Fine et al. (2002)
(conifers)	3.9-6.7	-	Fine et al. (2004)
	2.6-5.0	2.4-5.0	Engling et al. (2006)
	3.6-3.9	1.8-2.8	Schimidl et al. (2008)
Grasses	2.0-108.4	1.7-54.2	Oros et al. (2006); Engling et al. (2006); Kuo et al. (2001a)

As can be seen in Table 4, Oros et al., 2006 obtained levoglucosan to mannosan (L/M) and levoglucosan to sum of mannosan and galactosan (L/(M+G)) ratios between 2.0-33.3 and 1.7-9.5, respectively, while Engling et al.,

2006 detected a L/M and L/(M+G) ratios of 108.4 and 54.2 for different types of grasses. For softwood, Engling et al., 2006 obtained L/M and L/(M+G) ratios between 2.6-5.0 and 2.4-5.0, while Schmidl et al., 2008 reported 3.6-3.9 and 1.8-2.8, respectively. Kuo et al., 2011 detected, for 1 h, for cordgrass, L/M and L/(M+G) ratios of 24 and 3.7 (150 °C), 14.1 and 3.5 (200 °C), 36 and 12.7 (250 °C) and 29 and 14.5 (300 °C), respectively. Softwood generally gives the lowest L/M and L/(M+G) ratios than the others, e.g. the coniferous wood combustion L/M ratios is between 3-6, whereas hardwoods have higher ratios, e.g. the deciduous wood species whose L/M ratios values are between 15 and 23 (Engling et al., 2009). For the grasses, in all these studies, have the highest range and the highest ratios, except for the lignites because no galactosan was detected in the lignite smoke, compared to the other fuels (Kuo et al., 2011).

Fig. 20 shows the Paru Co's L/M and L/(M+G) ratios ranging from 0.6 to 100 and 0.5 to 11.1, respectively, and their oscillation throughout the Holocene, with the highest L/M value of ~100 and a very low L/(M+G) value of 1.7 in 6.6 ky BP, which may indicate the degradation of M and G due to their lower thermal stability. According to these values, predictions about the burnt vegetation can be made. The data show that grasses (GS) dominated the area from the beginning to the end of Paru Co's area and highlighted that softwoods (SW) began to live in the region after 10.74 ky BP. After it, GS, SW and hardwoods (HW) oscillated until 8.6 ky BP, when the vegetation was dominated by HW until 7.69 ky BP. Then, vegetation fluctuated again having the predominance of GS.

Since no standard literature data on the L/M and/or L/(M+G) ratios for any kind of fuels is available and nothing is known about the burning conditions and temperatures reached during the fires, it is quite difficult to precisely predict the vegetation type throughout the Holocene. In order to do that, the assumptions for the data obtained here were based on comparisons of the Holocene climate changes at Paru Co with other records from the Tibetan Plateau (Table 5 and Fig. 21).

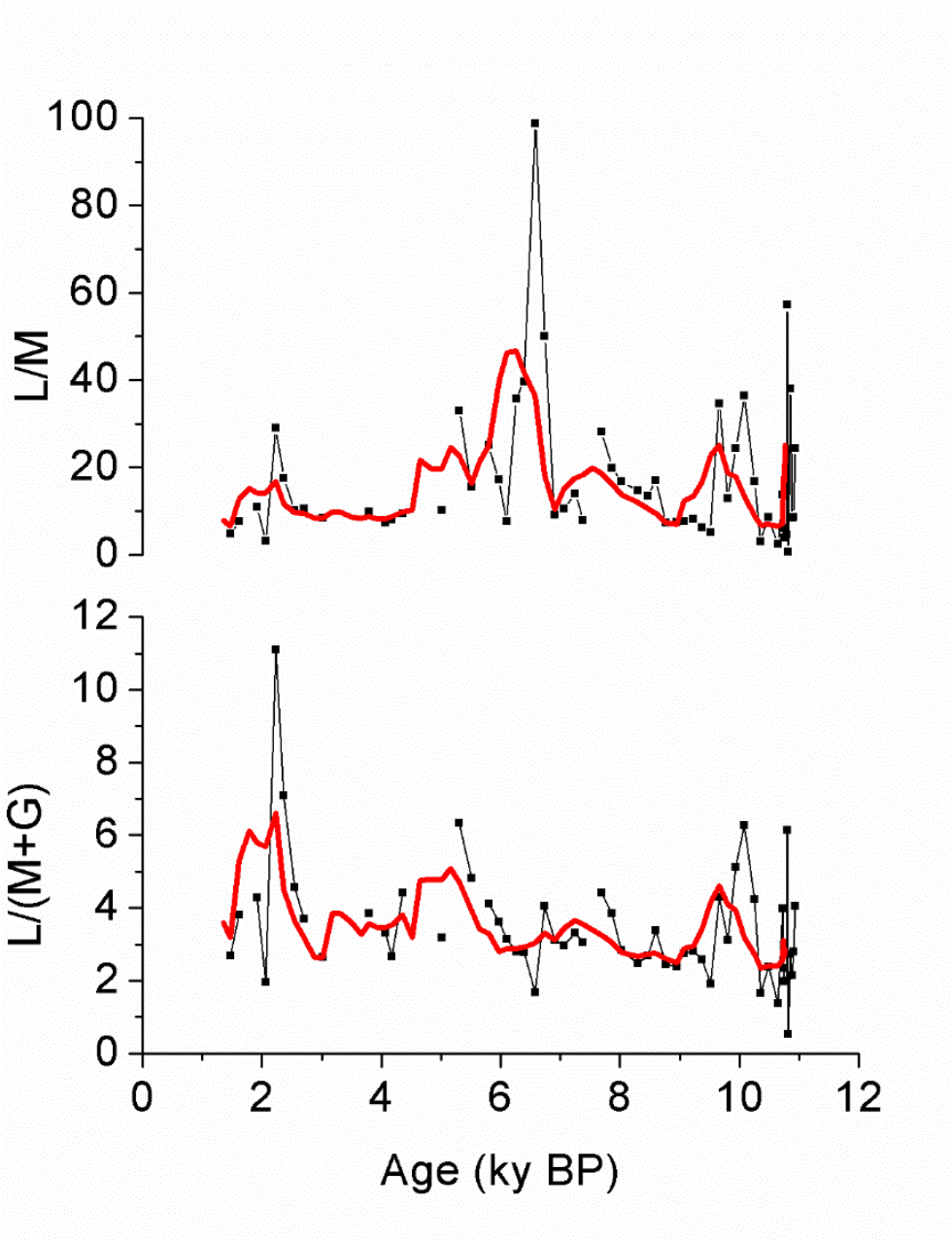

Fig. 20: Moving average and data points of levoglucosan to mannosan (L/M) and levoglucosan to the sum of mannosan and galactosan (L/(M+G)) ratios in Paru Co.

Table 5: Analysed lakes in the Tibetan Plateau, their geographic positions, and altitudes.

Lakes	Geographic Coordinates	Altitude (m a.s.l.)
Balikun Lake	43°36′-43°45′N, 92°42′-92°54′E	1,575
Bangong Co	33°40°N, 79°E	4,241
Bosten Lake	41°56’-42°14’N, 86°40’-87°26’E	1,048
Chen Co	28°53’-59’N, 90°33’-39’E	4,420
Cuoe Lake	31°24’-31°32’N, 91°28’-91°33’E	4,532
Erhai Lake	25.78°N, 100.19°E	1,972
Hidden Lake	29°48.77'N, 92°32.37'E	4,980
Hongyuan peat bog	32°46’N, 102°30’E	3,466
Hurleg Lake	37.17°N, 96.54°E,	2,817
Naleng Co	31.10°N, 99.75°E	4,200
Nam Co	30°30’-56’N, 90°16’-91°03’E	4,718
Paru Co	29.796°N, E 92.352°	4,845
Qinghai Lake	36°32’-37°15’N, 99°36’-100°47’E	3,200
Sayram Lake	44°30′-44°42′N, 81°05′-81°15′E	2,072
Seling Co	31.80°N, 89.01°E	4,530
Taro Co	31°03’-31°13’N, 83°55’-84°20’E	4,566
Tuolekule Lake	43°18′-43°23′N, 94°09′-94°16′ E	1,890
Wulungu Lake	46°59′-47°25′N, 87°00′-87°35′E	478.6
Zabuye Lake	31.35°N, 84.07°E	4,421
Zigetang Co	32.0°N, 90.9°E	4,560

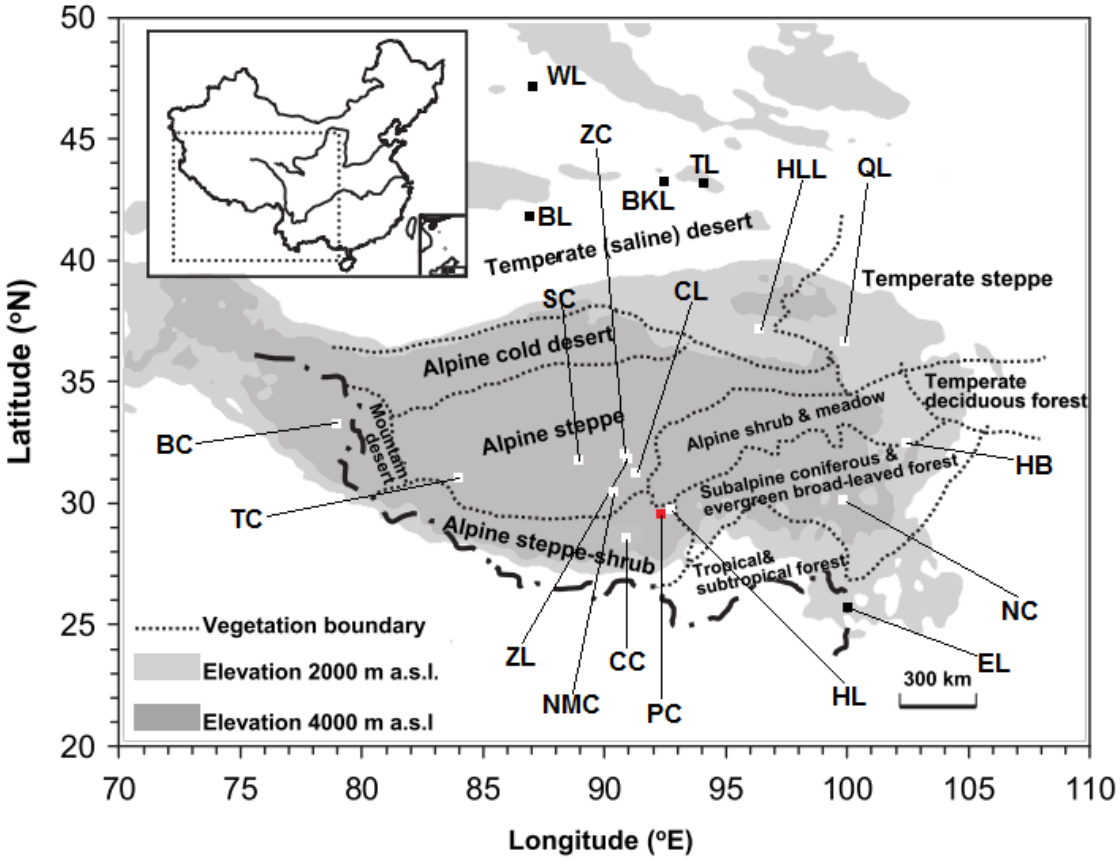

Fig. 21: Map of the Tibetan Plateau showing the regional vegetation and the location of sites mentioned in section 7.1.3. Paru Co (PC), Balikun Lake (BKL), Bangong Co (BC), Bosten Lake (BL), Chen Co (CC), Cuoe Lake (CL), Erhai Lake (EL), Hidden Lake (HL), Hongyuan peat bog (HB), Hurleg Lake (HLL), Naleng Co (NC), Nam Co (NMC), Qinghai Lake (QL), Sayram Lake (SL), Seling Co (SC), Taro Co (TC), Tuolekule Lake (TL), Wulungu Lake (WL), Zabuye Lake (ZL) and Zigetang Co (ZC). Adapted from Lu et al., 2011.

Pollen records obtained from Hidden Lake (HL, in Fig.20) have been divided into five pollen zones. Zone V (661-595 cm; 14-12.5 ky BP) was marked by high concentration of *Gramineae* (grass) and *Artemisia* (shrub) indicating the steppe vegetation. Between 12.5 and 9.2 ky BP (595-400 cm), meadow vegetation was present, mainly by *Cyperaceae* (grasslike herbaceous plants). From 9.2 to 3 ky BP (400-115 cm), trees such as *Betula* (trees and shrubs) and *Pinus* (conifer) began to live in the region, having their maximum between 7.2 and 5.3 ky BP,

followed by their decline from 5.3 to 3 ky BP (210-115 cm). Therefore, the fourth zone, from 12.5 to 7.3 ky BP was dominated by meadow and the third one, from 7.3 to 5.3, by forest. Zone II (5.3-3ky BP) shows that *Cyperaceae* and *Artemisia* increased, while *Betula* and *Pinus* declined, thus the vegetation converted to meadow. In the last zone, after 3 ky BP, *Artemisia* and *Gramineae* increased, and because of that, the vegetation changed into steppe. The climate shifted from cold-dry to warm-humid during the early Holocene and remained it until ~5 ky BP, followed by cold and dry conditions (Tang et al., 2000). Fig. 22 shows the pollen data found in Hidden Lake and the MA ratios obtained from Paru Co.

Pollen records from Chen Co Lake (CC in Fig. 21) have been divided into three zones. Zone III (1,250-1,040 cm; 10.7-9 ky BP) was marked by consistently and abundantly *Artemisia* pollens present throughout this zone with its percentage varying between 30% and 80%, while *Gramineae* pollen fluctuates between 5% and 20% with one peak (52.9%) at ca. 9.36 ky BP. *Cyperaceae* (grasslike herbaceous plants found especially in wet regions throughout the world) pollen declines sharply from 60% at the bottom to zero. This zone has high *Pinus* (max.31.6%) and *Chenopodiaceae* (mostly herbs and shrubs) (max.20%). The second zone (1,040-661 cm; 9.04-6.05 ky BP) has an abruptly increase in *Cyperaceae* pollen from 20% to 80%, whereas *Pinus*, *Chenopodiaceae*, *Gramineae*, and *Artemisia* pollen decreases significantly. *Umbelliferae* (herb) and *Betula* are more prevalent in this zone than in the others. Zone I (661-300 cm; 6.05-3.2 ky BP) is marked by an unsteadily decrease to low percentages (10-30%) in *Cyperaceae* pollen, while *Artemisia* pollen increases first, then by *Myriophyllum* (freshwater aquatic plants) which dramatically reached its highest levels (max. 53.3%) at ca. 5 ky BP. *Rosaceae* (herbs, shrubs, and trees) and *Composite* (herbs, shrubs, vines, and trees) pollen show a generally increasing trend. The climate between 10.7 and 9.04 ky BP was warm and dry, followed by a wet condition toward the mid-Holocene (9.04-6.05 ky BP) with a relatively humid phase around 8.6 ky BP, which explain why *Cyperaceae* pollen records dramatically fell from 60% to 0% in the third zone and then rose again, showing an upward trend in the second zone. After 7.2 ky, the climate became colder,

followed by a gradual decrease in pressure after 6.05, when the environment cooled rapidly (Lu et al., 2011; Zhu et al., 2009).

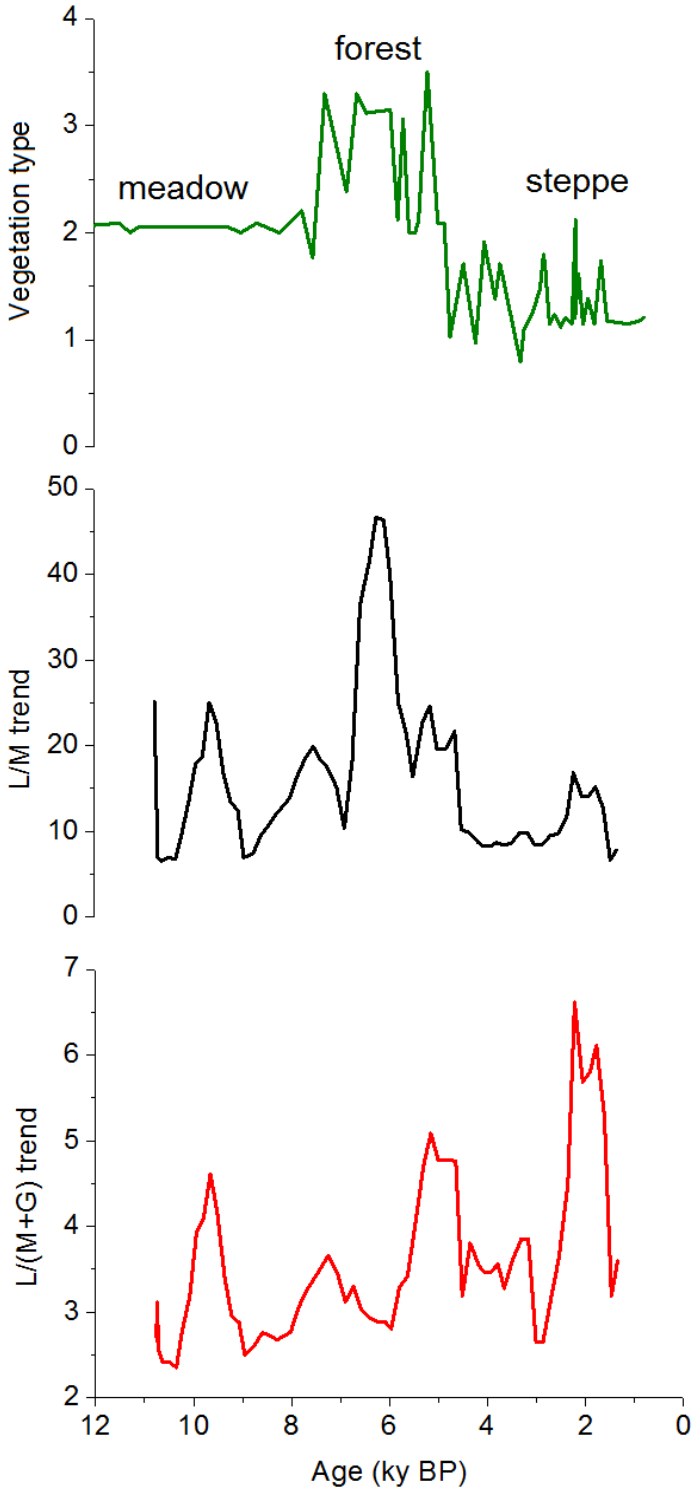

Fig. 22: A comparison between the vegetation type found in Hidden Lake from pollen records and the MAs trends found in Paru Co. a) type vegetation; b) L/M ratio trends; c) L/(M+G) ratios trends;

Pollen records from Taro Co, Naleng Co, Zigetang Co, Qinghai Lake and Seling Co showed that these regional climates changed from cold-dry to warm-humid, from 10.2 to 8.9 ky BP (Herzschuh et al., 2006; Kramer et al., 2010a,b; Ma et al., 2014). A decrease in the $\delta^{13}C$ values of cellulose in Hongyuan peat indicates the same climatic conditions, during the same period, which is probably due to a strong Indian Monsoon effect, like it happened to the regions mentioned before (Hong et al., 2003). At the same time, an increasing total tree pollen percentages from Qinghai Lake records accentuates that the climate tended to be warmer and wetter. Paru Co's results are in accordance with all this information, highlighting that the early Holocene climatic characteristics were mainly affected by the Indian Monsoon, which contributed with the inferred vegetation provided by the MA ratios (steppe to meadow and trees).

From 8.9 to 7.4 ky BP, a warm and humid climate was also hypothesised for explaining the pollen record at Hidden Lake and Naleng Co and from the records of multiple proxies at Erhai Lake (Ji et al., 2005; Kramer et al., 2010a, 2010b; Ma et al., 2014). However, in the westerlies domain, multiple proxies of the Wulungu Lake recorded a warm and dry climate between 10 and 7 ky BP as well as the Bosten Lake pollen record (Qingfeng et al., 2007; Wünnemann, Mischke, & Chen, 2006). A warm and dry environment registered a typical desert steppe/steppe vegetation at Saymram Lake from 9.6 to 5.5 ky BP (Qingfeng et al., 2013). Before 7.9 ky BP, Balikun Lake and Tuolekule Lake were characterized by the desert vegetation dominated by *Chenopodiaceae* and dry conditions (An et al., 2011a,b).

The transition zones of monsoon and westerlies were climatic inconsistent in the early Holocene. The Bangong Lake pollen record revealed warm and humid conditions, while Zabuye Lake records indicated warm and dry climate from 10.6 to 7.2 ky BP (Van Campo, Cour, & Sixuan, 1996; Wang et al., 2002). During 8.7–7.3 ky BP, the Zigetang Co data indicate that vegetation was sparse and the climate was dry (Herzschuh et al., 2006) as well as Hurleg Lake, in the northeastern Tibetan Plateau, whose results indicate dry conditions during 9.5–5.5 ky BP (Mischke & Zhang, 2010). From the beginning of the early Holocene, the temperature of the whole Tibetan Plateau revealed an increasing trend due

to a strong solar radiation in the northern hemisphere, which was similar to the climate records on the north Atlantic region (Berger & Loutre, 1991; Kaplan & Wolfe, 2006). On the contrary, this effect caused thermal differences between the land and sea and may have strengthened the monsoon with more precipitation in the transition zone of the monsoon and westerlies domain. Such information is strongly linked with the lithic data from Paru Co, because they suggest that ISM rainfall was enhanced between 10.1 and 7.1 ky BP. Inevitably, this caused the melting of ice and snow in the Tibetan Plateau, increasing the humidity in the monsoon domain during 8.9–7.4 ky BP (Chen et al., 2008). This may explain the highest levels of L, M and G from 11 to ~8 ky BP and also strongly support the values of L/M and L/(M+G) ratios found in the area, which show a fluctuation between grasses, softwoods and hardwoods until 8.6 ky BP, then a domination by HW until 7.7 ky BP (Fig.21a-b).

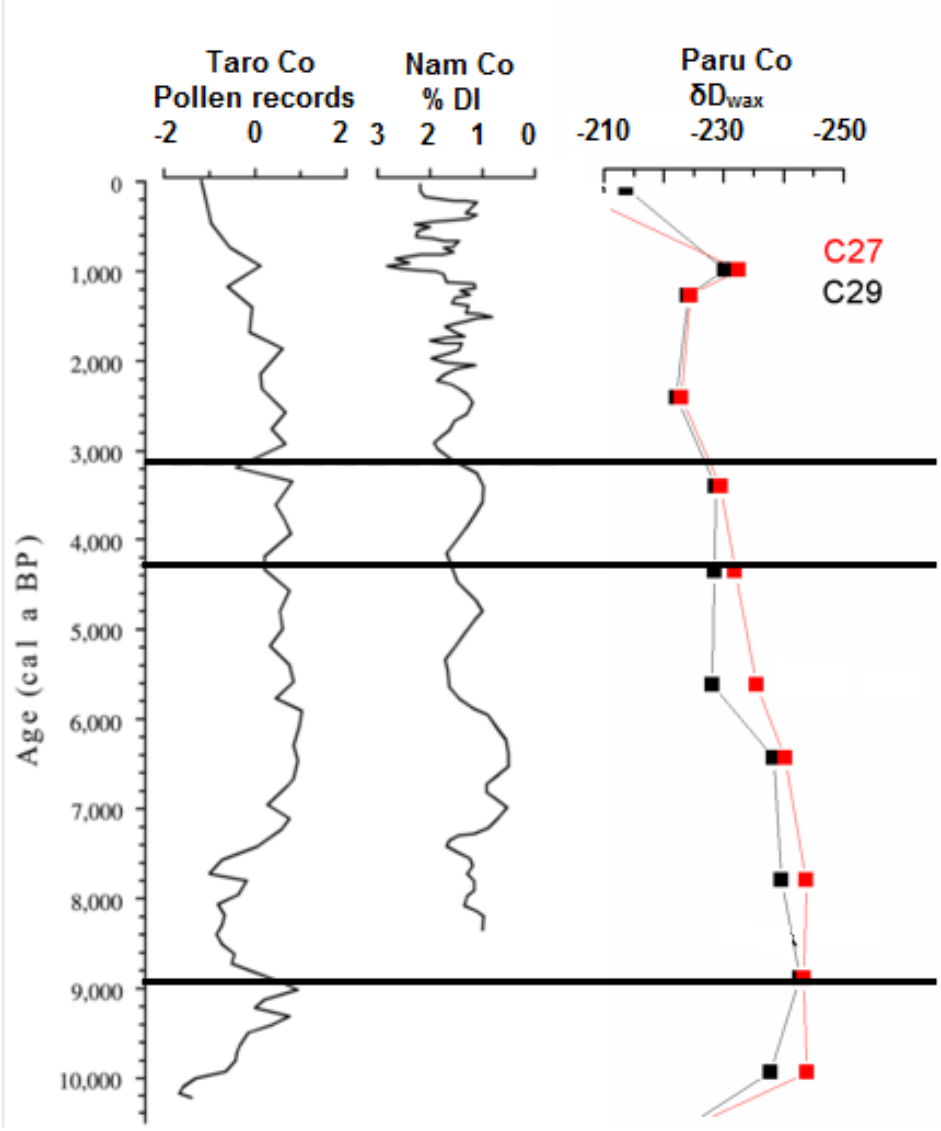

Fig. 23: Comparisons among Holocene changes at Paru Co and other lake sediment records. Result from fossil pollen data at Taro Co, sum of percentages of Chenopodiaceae, Cruciferae, Ephedra, Nitraria and Tamaricaceae from Nam Co record, and δD_{wax} results for the C-27 and C-29 n-alkanes at Paru Co. %DI stands for dryness index. Adapted from Ma et al., 2014.

Records from Taro Co, Nam Co, Zigetang Co, Cuoe Lake and Chen Co between 6.5-5.6, 7-6, 7.3-4.4, 8.6-5.7 and 9-6 ky BP, respectively, showed a warm and the wettest conditions throughout the Holocene. Records from Hidden

Lake also demonstrated that between 8-6 ky BP, Indian monsoon controlled the region and created wet conditions that withdrew the westerlies resulting in the disappearance of the ice sheet at high northern latitudes. These optimum climatic conditions are likely to be the best ones to plants grow, which may explain the peak in the ∑MAs in 6.6 ky BP by the presence of fires (Ji et al., 2005; Li et al., 2011; Ma et al., 2014; Yanhong et al., 2006; Zhu et al., 2009).

After the wettest period, the climate faced a gradual trend of increasing dryness. Records from many lakes in China showed a presence of an arid event at 4.3 ky BP. This occurrence did not take place only there, but also in other sites, such as the central North America, the Red Sea, the Mediterranean Sea, the Arabian Sea, India, and Africa (Arz, Lamy, & Pätzold, 2006; Booth et al., 2005; Enzel et al., 1999; Fleitmann, 2003; Gasse, 2000; Prasad & Enzel, 2006; Roberts et al., 2011). Solar variations, volcanic activity, the positioning of the equatorial convergence zone (ITCZ), and the changes in the surface sea temperature in the Pacific Ocean and the Atlantic Ocean are many of the hypothesis which may explain such event (Booth et al., 2005; Fleitmann et al., 2007; Gasse, 2000; Gupta, Das, & Anderson, 2005; Marchant & Hooghiemstra, 2004). Paru Co results are in agreement with records from the Mawmulh Cave, Ahung Co and Tianmen Cave records which suggest a coherent regional weakening in the ISM during the transition to the late Holocene (Morrill et al., 2003, Bird et al., 2014). Climatic changes in the North Atlantic region were also felt in the Tibetan Plateau by the westerlies, synchronised by the weakening of summer solar radiation in the northern hemisphere and the Indian Monsoon (Berger & Loutre, 1991; Fleitmann et al., 2007; Gupta et al., 2005; Overpeck et al., 1996). Nam Co and Taro Co, which are located in the same vegetation zone, recorded the influence by the westerlies during the late Holocene. From 5.6 to 0.9 ky BP, Paru Co's δD_{wax} increased suggesting a weakening in the ISM and a possible influence by the westerlies as well (Fig. 23) (Bird et al., 2014; Li et al., 2011; Ma et al., 2014). After 5 ky BP, temperature and precipitation decreased linearly and steppe vegetation began to degenerate(Tang et al., 2000).

The global charcoal database (GCD) contains information about paleofire activities by analysing charcoal records from sites across the globe since the last

glaciation maximum. Many of these studies can be found in the platform of GCD, which provides the scientific community a global paleofire dataset for research and archiving sedimentary records of fire. There is also a tool in R created by them called “paleofire: Analysis of Charcoal Records from the Global Charcoal Database”, which facilitates even more the access to analyse charcoal sedimentary data stored in the GCD (Blarquez et al., 2014). Main functionalities included data extraction and sites selection, transformation, and interpolation of the charcoal records as well as compositing. Choosing the latitude between 20-64° and longitude between 60-150°, data from 42 sites were collected as can be seen in Fig. 24.

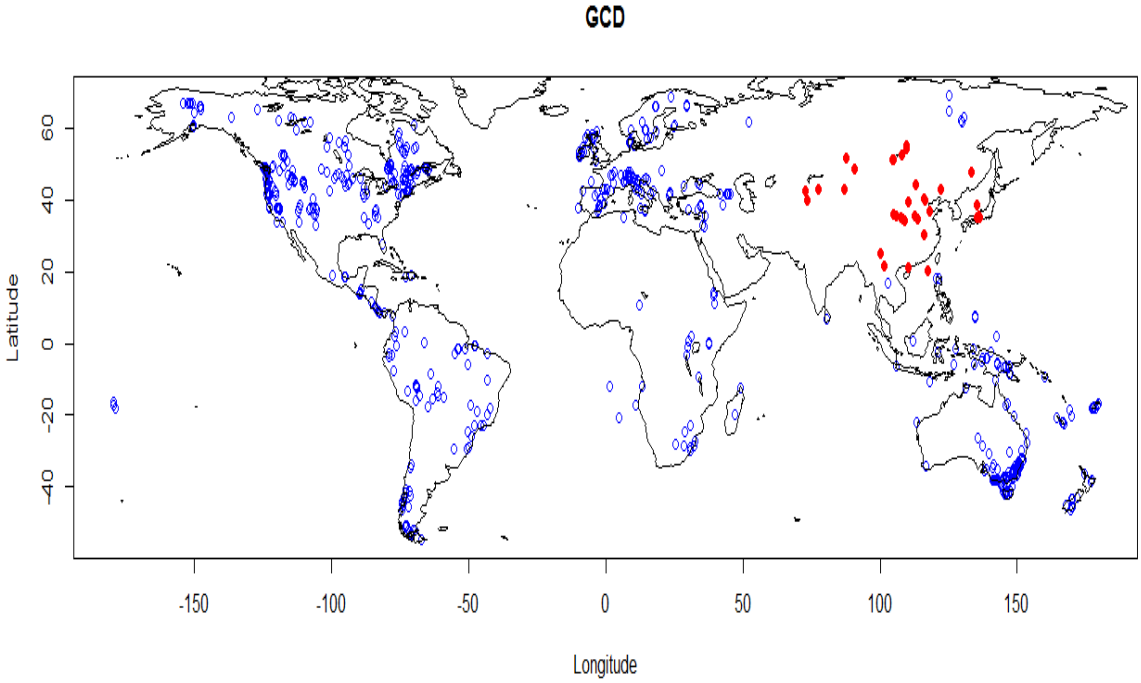

Fig. 24: World map with charcoal data from the paleofire R tool. Red dots represent the selected data between latitude 20-64° and longitude 60-150°.

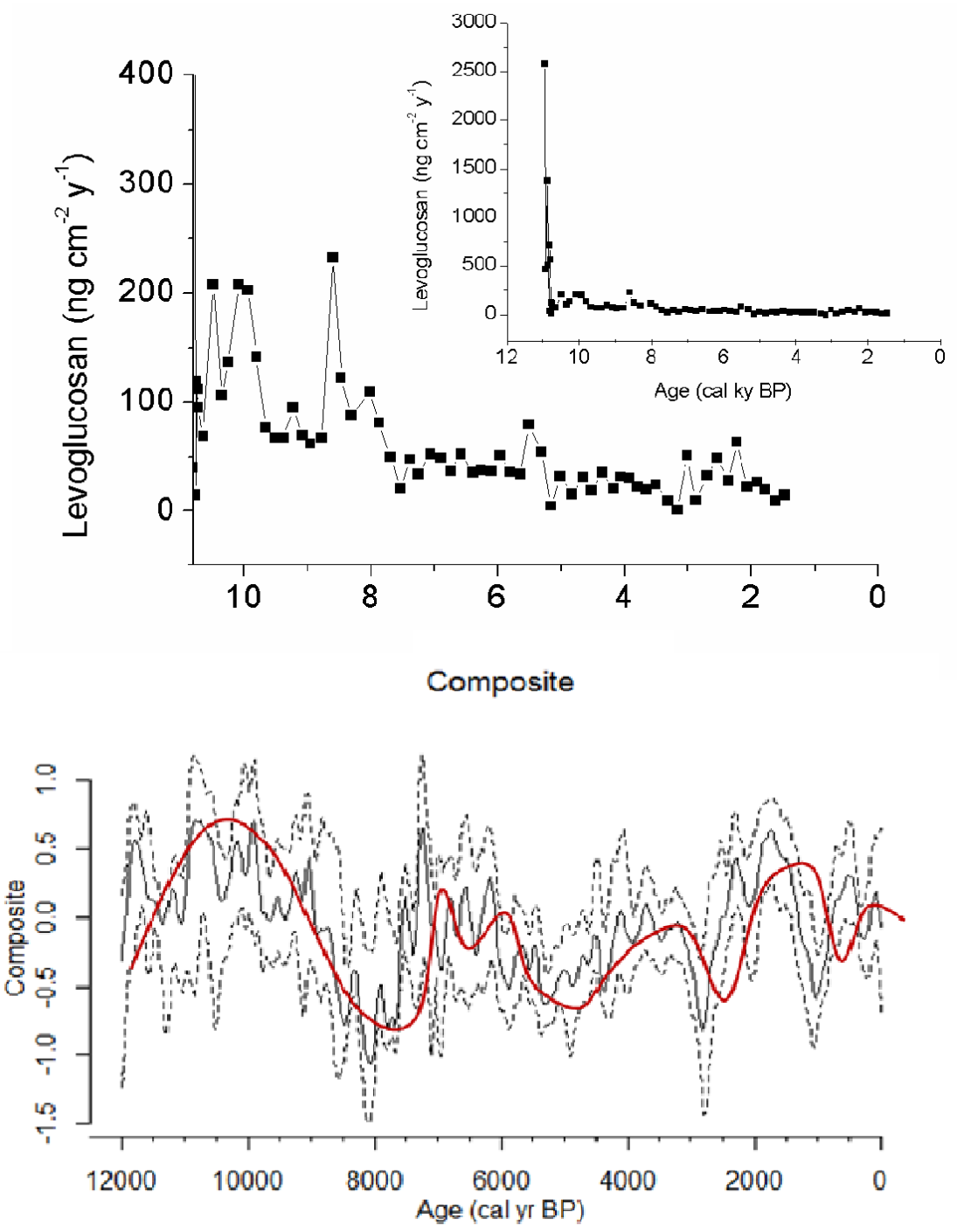

Fig. 25: Charcoal data transformation, background estimation and homogenisation for unique to multiple series from 42 sites compared to the fluxes of levoglucosan found in Paru Co.

As can be seen in Fig. 25, the sum of these 42 sites can prove that fire between 12-9 ky BP was in almost all these places when climate shifted from cold-dry to warm-wet. According to Marlon et al., 2013, many regions during the early Holocene were characterised by high fire, owing to local conditions, e.g. decreasing ice-sheet size, vegetation changes, and rising sea-surface temperature and sea level (Power et al., 2008). Records near glaciated regions, for example Canada, Alaska, and northeastern Europe show this pattern, as records from monsoon Asia. Such patterns likely reflect the influence of physical features (e.g., mountain ranges), storm tracks, shifts in monsoon conditions affecting vegetation communities and fir and/or the atmospheric circulation patterns during the early Holocene (Marlon et al., 2013)

Asia was marked by very low biomass burning ca 9-8 ky BP, while the opposite happened in Australasia at the same time. According to Bird et al., 2014, Paru Co was affected by the ISM, whose contributions were a warmer and wetter climate between ~11 and 5 ka, followed by a cooler and drier conditions after this time. The marked increase in fire between 6 and 5 ky BP, identified in individual records of charcoal, has been attributed to an increase in ENSO activity (Marlon et al., 2013). This information might be consistent with the increase in monosaccharide anhydride concentration in Paru Co ~5.5 ky BP.

6 CONCLUSION

Paru Co records provide an 11 ky BP wide perspective of the local and regional climate on the southeastern Tibetan Plateau. The seasonal variations of anhydrous sugars may be controlled by the East Asian and Indian Monsoon and the westerlies, which transport organic aerosols throughout the Tibetan Plateau. Overall, Indian Summer Monsoon rainfall was weaker between 11-10.7 ky BP, but rapidly strengthened until the mid-late Holocene. At the same time, warm-wet conditions at the early-mid Holocene were related to the Indian monsoon, and the cold-dry climate at mid-late Holocene was mainly caused by the westerlies. Thereby, the lake sedimentary record of Paru Co is important in order to further elaborate the impact by the Indian Monsoon or the Westerlies.

The results also revealed the suitability of MAs as a specific molecular marker for biomass burning in lake sediments. When integrated with multiple proxy records, MAs analyses have the potential to reconstruct not only the fire history on different spatial scales but also the whole environment itself. MA ratio is a very good tool to estimate changes in burnt fuels. When coupled with other proxies, e.g. pollen records, the outcomes demonstrate an optimistic relationship between them. The analyses of specific molecular markers and the analyses of additional proxies, such as PAHs, may help to discriminate if fire is local or not, and which kind of fuel has been burnt. However, this specific combination of proxies should be further investigated in future studies, because PAHs have uncertain sources and their degradation depends on several factors including: environmental conditions, number and type of the microorganisms, nature and chemical structure of the chemical compounds being degraded, etc.

Globally fire was low before the Holocene and increased in the beginning of the Holocene. This path coincides with the global increasing temperature through the glacial - interglacial transition. High fire activity matches with A) the widespread reorganisation of ecosystems that occurred in response to climate changes associated with deglaciation, and B) the dry conditions in Asia before 10 ky BP. The observed high levels of fire are consistent with early Holocene dry climate as well as biomass burning reduction in the following period. This

happens due to insolation-induced intensification of the Indian and Asian monsoons, showing wettest conditions ca 10-6 ky BP.

Even though several uncertainties still exist, the results of Paru Co demonstrate that the organic molecular markers (levoglucosan, mannosan and galactosan) have a high potential to provide fire information on different scales and changing fuel types. The inclusion of the MAs in a multi-proxy extraction method may improve the interpretation of drivers and sources of biomass burning.

7 BIBLIOGRAPHY

Abdel-Shafy, H. I., & Mansour, M. S. M. (2015). A review on polycyclic aromatic hydrocarbons: Source, environmental impact, effect on human health and remediation. *Egyptian Journal of Petroleum*, *25*(1), 107–123. https://doi.org/10.1016/j.ejpe.2015.03.011

An, C., Lu, Y., Zhao, J., Tao, S., Dong, W., Li, H., … Wang, Z. (2011). A high-resolution record of Holocene environmental and climatic changes from Lake Balikun (Xinjiang , China): Implications for central Asia. *The Holocene*, *22*, 43–52. https://doi.org/10.1177/0959683611405244

An, C., Zhao, J., Tao, S., Lv, Y., Dong, W., Li, H., … Wang, Z. (2011). Dust variation recorded by lacustrine sediments from arid Central Asia since ~ 15 cal ka BP and its implication for atmospheric circulation. *Quaternary Research*, *75*, 566–573. https://doi.org/10.1016/j.yqres.2010.12.015

Arz, H. W., Lamy, F., & Pätzold, J. (2006). A pronounced dry event recorded around 4.2 ka in brine sediments from the northern Red Sea. *Quaternary Research*, *66*(3), 432–441. https://doi.org/10.1016/j.yqres.2006.05.006

Battistel, D., Argiriadis, E., Kehrwald, N., Spigariol, M., Russell, J. M., & Barbante, C. (2016). Fire and human record at Lake Victoria , East Africa , during the Early Iron Age : Did humans or climate cause massive ecosystem changes ? https://doi.org/10.1177/0959683616678466

Berger, A., & Loutre, M. F. (1991). Insolation values for the climate of the last 10 million years. *Quaternary Science Reviews*, *10*(4), 297–317. https://doi.org/10.1016/0277-3791(91)90033-Q

Bird, B. W., Polisar, P. J., Lei, Y., Thompson, L. G., Yao, T., Finney, B. P., … Steinman, B. A. (2014). A Tibetan lake sediment record of Holocene Indian summer monsoon variability. *Earth and Planetary Science Letters*, *399*, 92–102. https://doi.org/10.1016/j.epsl.2014.05.017

Blarquez, O., Vannière, B., Marlon, J. R., Daniau, A. L., Power, M. J., Brewer, S., & Bartlein, P. J. (2014). Paleofire: An R package to analyse sedimentary charcoal records from the Global Charcoal Database to reconstruct past biomass burning. *Computers and Geosciences*, *72*, 255–261. https://doi.org/10.1016/j.cageo.2014.07.020

Bond, W. J. (2015). Fires in the Cenozoic: a late flowering of flammable ecosystems. *Frontiers in Plant Science*, *5*(January), 749. https://doi.org/10.3389/fpls.2014.00749

Booth, R. K., Jackson, S. T., Forman, S. L., Kutzbach, J. E., Bettis, E. a., Kreig, J., & Wright, D. K. (2005). A severe centennial-scale drought in midcontinental North America 4200 years ago and apparent global linkages. *The Holocene*, *15*, 321–328. https://doi.org/10.1191/0959683605hl825ft

Bowman, DM; Balch, JK; Artaxo, P; Bond, WJ; Carlson, JM; Cochrane, M., Antonio, CM; Defries, R., & Doyle, JC; Harrison, SP; Johnston, FH; Keeley, JE; Krawchuk, M. (2009). Fire in the Earth System. *Science*, *324*(April), 481–484. https://doi.org/10.1126/science.1163886

Bryden, K. M., & Hagge, M. J. (2003). Modeling the combined impact of moisture and char shrinkage on the pyrolysis of a biomass particle. *Fuel*, *82*(13), 1633–1644. https://doi.org/10.1016/S0016-2361(03)00108-X

Cerling, T. E., Harris, J. M., Macfadden, B. J., Leakey, M. G., Quadek, J., Eisenmann, V., & Ehleringer, J. R. (1997). Global vegetation change through the Miocene / Pliocene boundary. *Nature*, *389*, 153–158. https://doi.org/10.1038/38229

Chen, F., Yu, Z., Yang, M., Ito, E., Wang, S., Madsen, D. B., … Wünnemann, B. (2008). Holocene moisture evolution in arid central Asia and its out-of-phase relationship with Asian monsoon history. *Quaternary Science Reviews*, *27*(3–4), 351–364. https://doi.org/10.1016/j.quascirev.2007.10.017

Cole, J. (2001). Biomass Burning. Retrieved from http://earthobservatory.nasa.gov/Features/BiomassBurning/

Costa, M. S., Rego, A., Ramos, V., Afonso, T. B., Freitas, S., Preto, M., … Leão, P. N. (2016). The conifer biomarkers dehydroabietic and abietic acids are widespread in Cyanobacteria. *Scientific Reports*, *6*(November 2015), 23436. https://doi.org/10.1038/srep23436

Denis, E. H., Toney, J. L., Tarozo, R., Scott Anderson, R., Roach, L. D., & Huang, Y. (2012). Polycyclic aromatic hydrocarbons (PAHs) in lake sediments record historic fire events: Validation using HPLC-fluorescence detection. *Organic Geochemistry*, *45*, 7–17.

https://doi.org/10.1016/j.orggeochem.2012.01.005

Diessel, C. F. K. (2010). The stratigraphic distribution of inertinite. *International Journal of Coal Geology*, *81*(4), 251–268. https://doi.org/10.1016/j.coal.2009.04.004

Dong, H., Jiang, H., Yu, B., Liu, X., & Zhang, C. (2010). Impacts of environmental change and human activity on microbial ecosystems on the Tibetan Plateau, NW China. *GSA Today*, *20*(6), 4–10. https://doi.org/10.1130/GSATG75A.1

Dyurgerov, M. B., & Meier, M. F. (2005). Glaciers amd the Changing Earth System: A 2004 Snapshot. *Instaar*, (58).

Enache, M. D., & Cumming, B. F. (2006). Tracking recorded fires using charcoal morphology from the sedimentary sequence of Prosser Lake, British Columbia (Canada). *Quaternary Research*, *65*(2), 282–292. https://doi.org/10.1016/j.yqres.2005.09.003

Engling, G., Carrico, C. M., Kreidenweis, S. M., Collett, J. L., Day, D. E., Malm, W. C., … Herrmann, H. (2006). Determination of levoglucosan in biomass combustion aerosol by high-performance anion-exchange chromatography with pulsed amperometric detection. *Atmospheric Environment*, *40*(SUPPL. 2), 299–311. https://doi.org/10.1016/j.atmosenv.2005.12.069

Engling, G., Lee, J. J., Tsai, Y.-W., Lung, S.-C. C., Chou, C. C.-K., & Chan, C.-Y. (2009). Size-Resolved Anhydrosugar Composition in Smoke Aerosol from Controlled Field Burning of Rice Straw. *Aerosol Science and Technology*, *43*(7), 662–672. https://doi.org/10.1080/02786820902825113

Enzel, Y., Ely, L. L., Mishra, R., Ramesh, R., Amit, R., Lazar, B., … Sandler, A. (1999). High-Resolution Holocene Environmental Changes in the Thar Desert, Northwestern India. *Science*, *284*, 125–128.

Fabbri, D., Torri, C., Simoneit, B. R. T., Marynowski, L., Rushdi, A. I., & Fabianska, M. J. (2009). Levoglucosan and other cellulose and lignin markers in emissions from burning of Miocene lignites. *Atmospheric Environment*, *43*(14), 2286–2295. https://doi.org/10.1016/j.atmosenv.2009.01.030

Fleitmann, D. (2003). Holocene Forcing of the Indian Monsoon Recorded in a Stalagmite from Southern Oman. *Science*, *300*(5626), 1737–1739.

https://doi.org/10.1126/science.1083130

Fleitmann, D., Burns, S. J., Mangini, A., Mudelsee, M., Kramers, J., Villa, I., … Matter, A. (2007). Holocene ITCZ and Indian monsoon dynamics recorded in stalagmites from Oman and Yemen (Socotra). *Quaternary Science Reviews*, *26*(1–2), 170–188. https://doi.org/10.1016/j.quascirev.2006.04.012

Gasse, F. (2000). Hydrological changes in the African tropics since the Last Glacial Maximum. *Quaternary Science Reviews*, *19*(1–5), 189–211. https://doi.org/10.1016/S0277-3791(99)00061-X

Glasspool, I. J., Edwards, D., & Axe, L. (2006). Charcoal in the Early Devonian: A wildfire-derived Konservat-Lagerstätte. *Review of Palaeobotany and Palynology*, *142*(3–4), 131–136. https://doi.org/10.1016/j.revpalbo.2006.03.021

Glasspool, I. J., & Scott, A. C. (2010). Phanerozoic concentrations of atmospheric oxygen reconstructed from sedimentary charcoal. *Nature Geoscience*, *3*(9), 627–630. https://doi.org/10.1038/ngeo923

Gupta, A. K., Das, M., & Anderson, D. M. (2005). Solar influence on the Indian summer monsson during the Holocene. *Geophysical Research Letters*, *32*(17), 1–4. https://doi.org/10.1029/2005GL022685

Herzschuh, U., Winter, K., Wünnemann, B., & Li, S. (2006). A general cooling trend on the central Tibetan Plateau throughout the Holocene recorded by the Lake Zigetang pollen spectra. *Quaternary International*, *154–155*, 113–121. https://doi.org/10.1016/j.quaint.2006.02.005

Heyman, J. (2014). Palaeoglaciology of the northeastern Tibetan Plateau. *Quaternary Science Reviews*, *91*, 30–41. https://doi.org/10.1016/j.quascirev.2014.03.018

Hiltunen, M., Barišić, V., & Zabetta, E. C. (2008). Combustion of Different Types of Biomass in CFB Boilers-Foster Wheeler. *16th European Biomass Conference*, (April 2016), 6.

Hong, Y. T., Hong, B., Lin, Q. H., Zhu, Y. X., Shibata, Y., Hirota, M., … Yi, L. (2003). Correlation between Indian Ocean summer monsoon and North Atlantic climate during the Holocene. *Earth and Planetary Science Letters*, *211*(3–4), 371–380. https://doi.org/10.1016/S0012-821X(03)00207-3

Hopmans, E. C., dos Santos, R. A. L., Mets, A., Sinninghe Damsté, J. S., & Schouten, S. (2013). A novel method for the rapid analysis of levoglucosan in soils and sediments. *Organic Geochemistry*, *58*, 86–88. https://doi.org/10.1016/j.orggeochem.2013.02.003

Ji, S., Xingqi, L., Sumin, W., & Matsumoto, R. (2005). Palaeoclimatic changes in the Qinghai Lake area during the last 18,000 years. *Quaternary International*, *136*(1 SPEC. ISS.), 131–140. https://doi.org/10.1016/j.quaint.2004.11.014

Kaplan, M. R., & Wolfe, A. P. (2006). Spatial and temporal variability of Holocene temperature in the North Atlantic region. *Quaternary Research*, *65*(2), 223–231. https://doi.org/10.1016/j.yqres.2005.08.020

Kirchgeorg, T. (2015). Specific molecular markers in lake sediment cores for biomass burning reconstruction during the Holocene, 1–90.

Kirchgeorg, T., Schüpbach, S., Kehrwald, N., McWethy, D. B., & Barbante, C. (2014). Method for the determination of specific molecular markers of biomass burning in lake sediments. *Organic Geochemistry*, *71*, 1–6. https://doi.org/10.1016/j.orggeochem.2014.02.014

Kourtchev, I., Hellebust, S., Bell, J. M., O'Connor, I. P., Healy, R. M., Allanic, A., … Sodeau, J. R. (2011). The use of polar organic compounds to estimate the contribution of domestic solid fuel combustion and biogenic sources to ambient levels of organic carbon and PM2.5 in Cork Harbour, Ireland. *Science of the Total Environment*, *409*(11), 2143–2155. https://doi.org/10.1016/j.scitotenv.2011.02.027

Kramer, A., Herzschuh, U., Mischke, S., & Zhang, C. (2010a). Holocene treeline shifts and monsoon variability in the Hengduan Mountains (southeastern Tibetan Plateau), implications from palynological investigations. *Palaeogeography, Palaeoclimatology, Palaeoecology*, *286*(1–2), 23–41. https://doi.org/10.1016/j.palaeo.2009.12.001

Kramer, A., Herzschuh, U., Mischke, S., & Zhang, C. (2010b). Late glacial vegetation and climate oscillations on the southeastern Tibetan Plateau inferred from the Lake Naleng pollen profile. *Quaternary Research*, *73*(2), 324–335. https://doi.org/10.1016/j.yqres.2009.12.003

Kuo, L. J., Louchouarn, P., & Herbert, B. E. (2011). Influence of combustion

conditions on yields of solvent-extractable anhydrosugars and lignin phenols in chars: Implications for characterizations of biomass combustion residues. *Chemosphere*, *85*(5), 797–805. https://doi.org/10.1016/j.chemosphere.2011.06.074

Lakshmanan, C. M., & Hoelscher, H. E. (1970). Production of Levoglucosan by Pyrolysis of Carbohydrates - Pyrolysis in Hot Inert Gas Stream. *Ind. Eng. Chem. Prod. Res. Develop.*, *9*(1), 57–59. https://doi.org/10.1002/star.19700220804

Lammel, G., Sehili, A. M., Bond, T. C., Feichter, J., & Grassl, H. (2009). Chemosphere Gas / particle partitioning and global distribution of polycyclic aromatic hydrocarbons – A modelling approach. *Chemosphere*, *76*(1), 98–106. https://doi.org/10.1016/j.chemosphere.2009.02.017

Lehmkuhl, F., Owen, L. a, & Derbyshire, E. (1998). Late Quaternary glacial history of northeast Tibet. *Journal of Quaternary Science*.

Li, Q., Lu, H., Zhu, L., Wu, N., Wang, J., & Lu, X. (2011). Pollen-inferred climate changes and vertical shifts of alpine vegetation belts on the northern slope of the Nyainqentanglha Mountains (central Tibetan Plateau) since 8.4 kyr BP. *The Holocene*, *21*(6), 939–950. https://doi.org/10.1177/0959683611400218

Liu, H., Cui, Y., Zuo, X., Li, H., Wang, J., Zhang, D., … Dong, G. (2015). Human settlements and plant utilization since the late prehistoric period in the Nujiang River valley, Southeast Tibetan Plateau. *Archaeological Research in Asia*, (August). https://doi.org/10.1016/j.ara.2016.02.002

Liu, W., Zhang, Z., & Wan, S. (2009). Predominant role of water in regulating soil and microbial respiration and their responses to climate change in a semiarid grassland. *Global Change Biology*, *15*(1), 184–195. https://doi.org/10.1111/j.1365-2486.2008.01728.x

Lu, H., Wu, N., Liu, K. biu, Zhu, L., Yang, X., Yao, T., … Jiang, H. (2011). Modern pollen distributions in Qinghai-Tibetan Plateau and the development of transfer functions for reconstructing Holocene environmental changes. *Quaternary Science Reviews*, *30*(7–8), 947–966. https://doi.org/10.1016/j.quascirev.2011.01.008

Lynch, E. A., Hotchkiss, S. C., & Calcote, R. (2011). Charcoal signatures defined by multivariate analysis of charcoal records from 10 lakes in northwest Wisconsin (USA). *Quaternary Research*, *75*(1), 125–137. https://doi.org/10.1016/j.yqres.2010.08.007

Ma, Q., Zhu, L., L, X., Guo, Y., Ju, J., Wang, J., … Tang, L. (2014). Pollen-inferred Holocene vegetation and climate histories in Taro Co, southwestern Tibetan Plateau. *Chinese Science Bulletin*, *59*(31), 4101–4114. https://doi.org/10.1007/s11434-014-0505-1

Marchant, R., & Hooghiemstra, H. (2004). Rapid environmental change in African and South American tropics around 4000 years before present: A review. *Earth-Science Reviews*, *66*(3–4), 217–260. https://doi.org/10.1016/j.earscirev.2004.01.003

Marlon, J. R., Bartlein, P. J., Daniau, A. L., Harrison, S. P., Maezumi, S. Y., Power, M. J., … Vannière, B. (2013). Global biomass burning: A synthesis and review of Holocene paleofire records and their controls. *Quaternary Science Reviews*, *65*, 5–25. https://doi.org/10.1016/j.quascirev.2012.11.029

Mckendry, P. (2002). Energy production from biomass (part 1): overview of biomass, *83*(July 2001), 37–46.

Miao, Y., Fang, X., Song, C., Yan, X., Zhang, P., Meng, Q., … Wang, Y. (2016). Late Cenozoic fire enhancement response to aridification in mid-latitude Asia: Evidence from microcharcoal records. *Quaternary Science Reviews*, *139*(March), 53–66. https://doi.org/10.1016/j.quascirev.2016.02.030

Mischke, S., & Zhang, C. (2010). Holocene cold events on the Tibetan Plateau. *Global and Planetary Change*, *72*(3), 155–163. https://doi.org/10.1016/j.gloplacha.2010.02.001

Northup, B. K., Zitzer, S. F., Archer, S., McMurtry, C. R., & Boutton, T. W. (2005). Above-ground biomass and carbon and nitrogen content of woody species in a subtropical thornscrub parkland. *Journal of Arid Environments*, *62*(1), 23–43. https://doi.org/10.1016/j.jaridenv.2004.09.019

Oros, D. R., Abas, M. R. bin, Omar, N. Y. M. J., Rahman, N. A., & Simoneit, B. R. T. (2006). Identification and emission factors of molecular tracers in organic aerosols from biomass burning: Part 3. Grasses. *Applied*

Geochemistry, *21*(6), 919–940. https://doi.org/10.1016/j.apgeochem.2006.01.008

Overpeck, J., Anderson, D., Trumbore, S., & Prell, W. (1996). The southwest Indian Monsoon over the last 18 000 years. *Climate Dynamics*, *12*, 213–225. https://doi.org/10.1007/BF00211619

Patel, B., & Gami, B. (2012). Biomass Characterization and its Use as Solid Fuel for Combustion. *Iranica Journal of Energy & Environment*, *3*(2), 123–128. https://doi.org/10.5829/idosi.ijee.2012.03.02.0071

Pausas, J. G., & Keeley, J. E. (2009). A burning story: The role of rire in the history of life. *BioScience*, *59*(7), 593–601. https://doi.org/10.1525/bio.2009.59.7.10

Perez, J., Muñoz-Dorado, J., Martıinez, J., & de la Rubia, T. (2002). Biodegradation and biological treatments of cellulose , hemicellulose and lignin : an overview, 53–63. https://doi.org/10.1007/s10123-002-0062-3

Power, M. J., Marlon, J., Ortiz, N., Bartlein, P. J., Harrison, S. P., Mayle, F. E., … Zhang, J. H. (2008). Changes in fire regimes since the last glacial maximum: An assessment based on a global synthesis and analysis of charcoal data. *Climate Dynamics*, *30*(7–8), 887–907. https://doi.org/10.1007/s00382-007-0334-x

Prasad, S., & Enzel, Y. (2006). Holocene paleoclimates of India. *Quaternary Research*, *66*(3), 442–453. https://doi.org/10.1016/j.yqres.2006.05.008

Qingfeng, J., Ji, S., Xingqi, L. I. U., Enlou, Z., & Xiayun, X. (2007). A high-resolution climatic change since Holocene inferred from multi-proxy of lake sediment in westerly area of China, *52*(40625007). https://doi.org/10.1007/s11434-007-0245-6

Qingfeng, J., Junfeng, J. I., Ji, S., Matsumoto, R., Guobang, T., Peng, Q., … Dezhi, Y. A. N. (2013). Holocene vegetational and climatic variation in westerly- dominated areas of Central Asia inferred from the Sayram Lake in northern Xinjiang , China, *56*(3), 339–353. https://doi.org/10.1007/s11430-012-4550-9

Roberts, N., Eastwood, W. J., Kuzucuoglu, C., Fiorentino, G., & Caracuta, V. (2011). Climatic, vegetation and cultural change in the eastern

Mediterranean during the mid-Holocene environmental transition. *The Holocene*, *21*(1), 147–162. https://doi.org/10.1177/0959683610386819

Schmidl, C., Marr, I. L., Caseiro, A., Kotianová, P., Berner, A., Bauer, H., … Puxbaum, H. (2008). Chemical characterisation of fine particle emissions from wood stove combustion of common woods growing in mid-European Alpine regions. *Atmospheric Environment*, *42*(1), 126–141. https://doi.org/10.1016/j.atmosenv.2007.09.028

Schüpbach, S., Kirchgeorg, T., Colombaroli, D., Beffa, G., Radaelli, M., Kehrwald, N. M., & Barbante, C. (2015). Combining charcoal sediment and molecular markers to infer a Holocene fire history in the Maya Lowlands of Petén, Guatemala. *Quaternary Science Reviews*, *115*, 123–131. https://doi.org/10.1016/j.quascirev.2015.03.004

Scott, A. . (2000). The Pre-Quaternary history of fire. *Palaeogeography, Palaeoclimatology, Palaeoecology*, *164*(1–4), 281–329. https://doi.org/10.1016/S0031-0182(00)00192-9

Severinghaus, J. P., & Brook, E. J. (1999). Abrupt Climate Change at the End of the Last Glacial Period Inferred from Trapped Air in Polar Ice. *Science*, *286*(October), 930–933. https://doi.org/10.1126/science.286.5441.930

Shearer, J. C., Moore, T. A., & Demchuk, T. D. (1995). Delineation of the distinctive nature of tertiary coal beds. *International Journal of Coal Geology*, *28*(2–4), 71–98. https://doi.org/10.1016/0166-5162(95)00014-3

Simoneit, B. R. T. (2002). *Biomass burning - A review of organic tracers for smoke from incomplete combustion*. *Applied Geochemistry* (Vol. 17). https://doi.org/10.1016/S0883-2927(01)00061-0

Stier, P., Feichter, J., Kinne, S., Kloster, S., Vignati, E., Wilson, J., … Petzold, A. (2005). The aerosol-climate model ECHAM5-HAM. *Atmospheric Chemistry and Physics*, *5*(4), 1125–1156. https://doi.org/10.5194/acp-5-1125-2005

Stogiannidis, E., & Laane, R. (2013). *Source Characterization of Polycyclic Aromatic Hydrocarbons by Using Their Molecular Indices: An Overview of Possibilities*. *Introduction to Partial Differential Equations* (Vol. 234). https://doi.org/10.1007/978-3-

Tang, L., Shen, C., Liu, K., & Overpeck, J. T. (2000). Changes in South Asian

monsoon : New high-resolution paleoclimatic records from Tibet , China. *Chinese Science Bulletin*, *45*(1), 87–91. https://doi.org/10.1007/BF02884911

Van Campo, E., Cour, P., & Sixuan, H. (1996). Holocene environmental changes in Bangong Co basin (Western Tibet). Part 2: The pollen record. *Palaeogeography, Palaeoclimatology, Palaeoecology*, *120*(1â€“2), 49–63. https://doi.org/10.1016/0031-0182(95)00033-x

Verma, M., Loha, C., Sinha, A. N., & Chatterjee, P. K. (2017). Drying of biomass for utilising in co-firing with coal and its impact on environment – A review. *Renewable and Sustainable Energy Reviews*, *71*(February 2015), 732–741. https://doi.org/10.1016/j.rser.2016.12.101

Wang, R. L., Scarpitta, S. C., Zhang, S. C., & Zheng, M. P. (2002). Later Pleistocene/Holocene climate conditions of Qinghai-Xizhang Plateau (Tibet) based on carbon and oxygen stable isotopes of Zabuye Lake sediments. *Earth and Planetary Science Letters*, *203*(1), 461–477. https://doi.org/10.1016/S0012-821X(02)00829-4

Whitlock, C., & Larsen, C. P. S. (2001). Charcoal as a Fire Proxy. *Tracking Environmental Change Using Lake Sediments.*, *Volume 3:T*, 557–578. https://doi.org/10.1007/978-94-007-2745-8

Wünnemann, B., Mischke, S., & Chen, F. (2006). A Holocene sedimentary record from Bosten Lake , China, *234*, 223–238. https://doi.org/10.1016/j.palaeo.2005.10.016

Xu, J., Shrestha, A., Vaidya, R., Eriksson, M., & Hewitt, K. (2007). The melting Himalayas: regional challenges and local impacts of climate change on mountain ecosystems and livelihoods. *The Melting Himalayas: Regional Challenges and Local Impacts of Climate Change on Mountain Ecosystems and Livelihoods*, vi--. https://doi.org/10.1111/j.1523-1739.2009.01237.x

Yang, H., Yan, R., Chen, H., Lee, D. H., & Zheng, C. (2007). Characteristics of hemicellulose, cellulose and lignin pyrolysis. *Fuel*, *86*(12–13), 1781–1788. https://doi.org/10.1016/j.fuel.2006.12.013

Yang, H., Yan, R., Chen, H., Zheng, C., Lee, D. H., Uni, V., … September, V. (2006). In-Depth Investigation of Biomass Pyrolysis Based on Three Major

Components : Hemicellulose , Cellulose and Lignin, (17), 388–393.

Yang, R., Xie, T., Li, A., Yang, H., Turner, S., Wu, G., & Jing, C. (2016). Sedimentary records of polycyclic aromatic hydrocarbons (PAHs) in remote lakes across the Tibetan Plateau. *Environmental Pollution*, *214*(April), 1–7. https://doi.org/10.1016/j.envpol.2016.03.068

Yanhong, W., Lücke, A., Zhangdong, J., Sumin, W., Schleser, G. H., Battarbee, R. W., & Weilan, X. (2006). Holocene climate development on the central Tibetan Plateau: A sedimentary record from Cuoe Lake. *Palaeogeography, Palaeoclimatology, Palaeoecology*, *234*(2–4), 328–340. https://doi.org/10.1016/j.palaeo.2005.09.017

YI, C., CHEN, H., YANG, J., LIU, B., FU, P., LIU, K., & LI, S. (2008). Review of Holocene glacial chronologies based on radiocarbon dating in Tibet and its surrounding mountains. *Journal of Quaternary Science*, *23*(6–7), 533–543. https://doi.org/10.1002/jqs

You, C., Yao, T., Gao, S., Gong, P., & Zhao, H. (2014). Simultaneous determination of levoglucosan, mannosan and galactosan at trace levels in snow samples by GC/MS. *Chromatographia*, *77*(13–14), 969–974. https://doi.org/10.1007/s10337-014-2702-0

Zakir Hossain, H. M., Sampei, Y., & Roser, B. P. (2013). Polycyclic aromatic hydrocarbons (PAHs) in late Eocene to early Pleistocene mudstones of the Sylhet succession, NE Bengal Basin, Bangladesh: Implications for source and paleoclimate conditions during Himalayan uplift. *Organic Geochemistry*, *56*, 25–39. https://doi.org/10.1016/j.orggeochem.2012.12.001

Zennaro, P., Kehrwald, N., McConnell, J. R., Schüpbach, S., Maselli, O. J., Marlon, J., … Barbante, C. (2014). Fire in ice: Two millennia of boreal forest fire history from the Greenland NEEM ice core. *Climate of the Past*, *10*(5), 1905–1924. https://doi.org/10.5194/cp-10-1905-2014

Zheng, B., & Rutter, N. (1998). On the problem of Quaternary glaciations, and the extent and patterns of Pleistocene ice cover in the Qinghai-Xizang (Tibet) Plateau. *Quaternary International*, *45–46*(97), 109–122. https://doi.org/10.1016/S1040-6182(97)00009-8

Zhou, B., Shen, C., Sun, W., Zheng, H., Yang, Y., Sun, Y., & An, Z. (2007).

Elemental carbon record of paleofire history on the Chinese Loess Plateau during the last 420 ka and its response to environmental and climate changes. *Palaeogeography, Palaeoclimatology, Palaeoecology*, *252*(3–4), 617–625. https://doi.org/10.1016/j.palaeo.2007.05.014

Zhu, L., Zhen, X., Wang, J., Lü, H., Xie, M., Kitagawa, H., & Possnert, G. (2009). A ~30,000-year record of environmental changes inferred from Lake Chen Co, Southern Tibet. *Journal of Paleolimnology*, *42*(3), 343–358. https://doi.org/10.1007/s10933-008-9280-9